Development of a laser ionization test bench for radioactive ion beams

by

Lucky M Makhathini

Submitted to the Faculty of Science and Agriculture in partial fulfilment of the requirements for the degree of Masters of Science in the Department of Physics at University of Zululand

Supervisor: Dr. R. A. Bark

iThemba LABS, Old Faure Rd

Faure, South Africa

Co-supervisors: Prof O. M. Ndwandwe

University of Zululand, Faculty of science and Agriculture

Department of physics, Private Bag X1001

KwaDlangezwa, 3886

February 2013

Declaration

By submitting this thesis, I declare that the entirety of the work contained therein is my own, original work, (that I am the owner of the copyright thereof unless to the extent explicitly otherwise stated) and that I have not previously in its entirety or in part submitted it for obtaining any qualification.

Abstract

This thesis aims to develop the technique for selective laser ionization of atoms and the role it can play in the production of radioactive ion beams. The theory of the production of radioactive ion beams and resonant laser ionization using different techniques will be discussed. Furthermore, the Isotope Separation On-Line method will be comprehensively discussed and the requirements needed for the development of a laser ion source will be summarized. The selective laser ionization of atoms will be demonstrated using using two different techniques, laser-enhanced ionization in gas and using a time-of-flight mass spectrometer.

In laser-enhanced ionization in gas, atoms will be ejected into a flame via a device called a nebulizer where the atoms will be excited by two-step excitation followed by collisional ionization in the flame. The signal obtained will be fed onto a "boxcar" for data processing and analysing. In time-of-flight mass spectroscopy, a collimated beam of stable atoms will be created and the detailed design and construction of the atomic beam source and the time-of-flight mass spectrometer will be shown. Two-step ionization of atoms will be used to ionize the created beam and and the ionized atoms will be accelerated twice by electric fields, after which they will enter a free-field region and they will be separated according to their mass to charge ratio. The interpretation of the results obtained will conclude the thesis and future prospects for the project will be given.

Dedication

Dedicated to my mother, Benzile Goodness Duma

Acknowledgements

My gratitude to the following people:

God for guiding and protecting me through all the ups and downs of the whole project via Philippians 4:13 "I can do all things through Christ who strengthens me"

Members of MANuS/MatSci (Masters in Accelerator and Nuclear/Material Sciences) programme at the University of Zululand and University of the Western Cape, iThemba LABS, and Stellenbosch University for providing me with such an outstanding study opportunity.

Dr. R.A. Bark for his brilliant supervision and guidance of this work and for countless discussions which have contributed to the success of this project.

Prof. P.E. Walters for facilitated my first steps in the field of laser ionization and discussions about the experimental work and guidance.

Prof E.G. Rohwer for making sure that I got everything I needed for my practical work.

Dr. J.C. Cornell for his comments on the manuscript and for his suggestions for further reading.

Dr. P. Papka for assisting in designing the atomic beam source.

The Stellenbosch technical team, Mr Ulli Deutschlander, Mr John Germishuizer and Mr Gerard Louwrens for help with practical aspects of the work: my sincere thanks to them all.

iThemba LABS workshop group for building our atomic beam source and for being there whenever I needed them to do the mechanical work.

All members of the Laser Research Institute for their advice.

My family and friends, for love, support, motivation and understanding.

Contents

List of Figures

List of Tables

Chapter 1

Introduction

1.1 Motivation

Selective ionization of atoms can be of great importance since it can produce an uncontaminated radioactive beam. Using selective ionization of atoms produced in nuclear reactions (e.g fission of uranium) can make it easy to ionize only the specific element of interest.

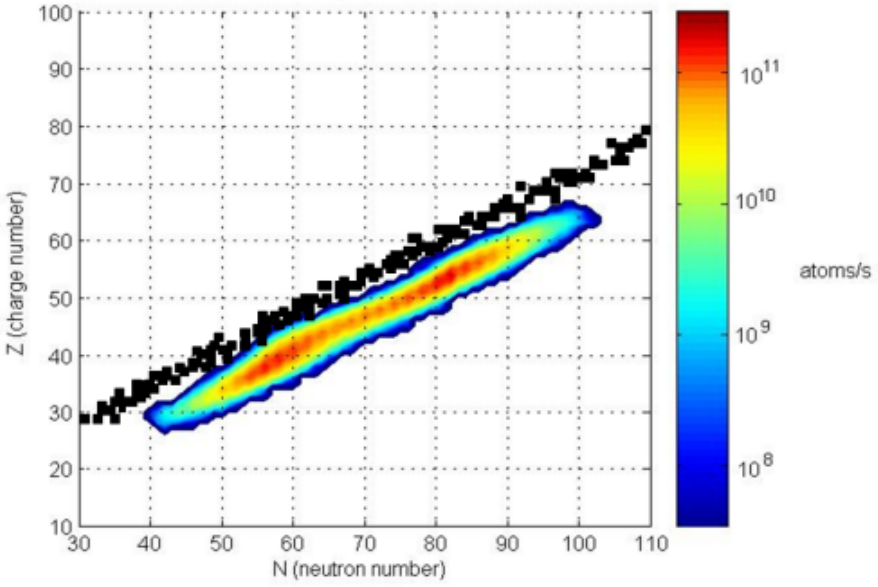

FIG. 1.1. The isotope yield from a nuclear fission reaction [1].

Fission of uranium produces hundreds of different species as shown in figure 1.1, consequently, we need a technique to allow us to select a species in particular. The other ionization methods that are currently used (surface and electron-impact ionization) are not especially selective. With laser ionization using a tunable laser, we can tune the output wavelength to match the specific transition of any atom. This makes it easy to ionize it and to extract it by applying an electric field.

1.2 Aim

The main aim of the work documented in this dissertation is to develop a resonance laser ionization test-bench for radioactive ion beams. To develop this technique we will start by demonstrating selective ionization of a stable beam of atoms. We will first demonstrate laser ionization in air before proceeding to the next level of complexity to selectivity ionize atoms in a vacuum. Ionizing strontium atoms in air will be demonstrated by measuring the current produced as result of laser ionization. The second aim is to ionize indium in vacuum using a time-of-flight mass spectrometer to confirm that indium atoms were indeed selectively ionized as result of laser ionization.

1.3 Radioactive ion beams

The interest in studies of nuclei that lie far away from the stability line has led to the development of accelerator facilities to produce radioactive ion beams. This interest led to development of the new facilities for producing RIBs around the globe. The principal interest in RIBs is that it will provide new knowledge for nuclear and astrophysics research and will also increase the number of nuclei that can be studied, especially nuclei with extreme values of the neutron-to-proton ratio (N/Z) [2]. Much of the nuclear information known so far is from nuclei near the valley of stability, or which were produced by stable beams on stable targets. Accelerated RIBs gives access to new regions of proton- and neutron-rich nuclei, giving new exciting opportunities for research in nuclear physics, astrophysics and other field of scientific research.

1.3.1 Importance and Application

The main importance of radioactive beam is for extending our understanding of the atomic nucleus. However, having intense beam of certain radioactive isotopes can be extremely useful in other fields of research as shown in figure 1.2. Some of the applications are elaborated in the following topics such as studying fundamental interactions (nuclear physics), nuclear astrophysics, materials science and medical physics.

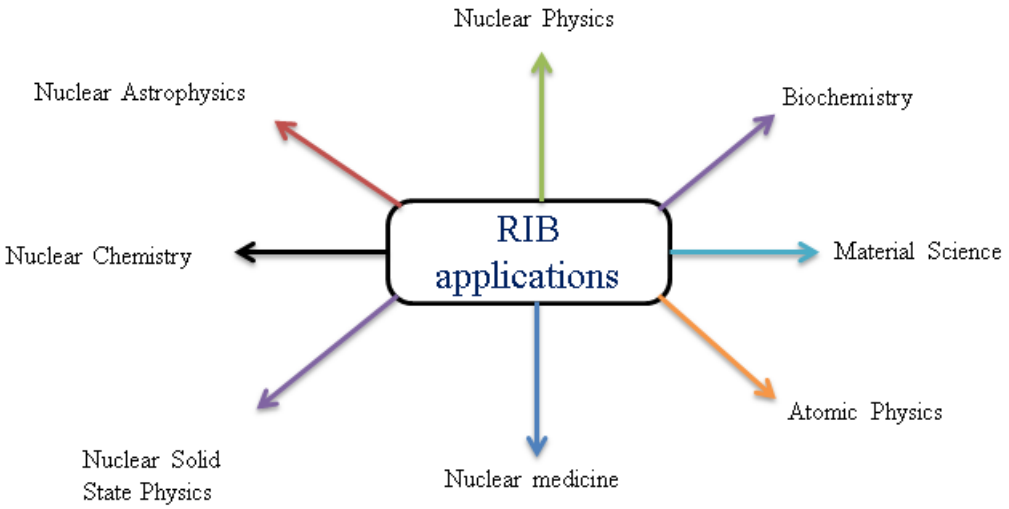

FIG. 1.2. Applications of radioactive-ion beams in the field of science.

Nuclear Physics

Figure 1.3 shows the chart of the nuclides: the naturally occurring nuclei are in black, those that have been artificially produced are shown in yellow and these comprise approximately half of all the species that are predicted to exist. The unknown nucleid are shown in the green region and they lie mainly on the neutron-rich side of the naturally occurring isotopes and, even for known neutron-rich nuclei, very little information is known other than their existence.

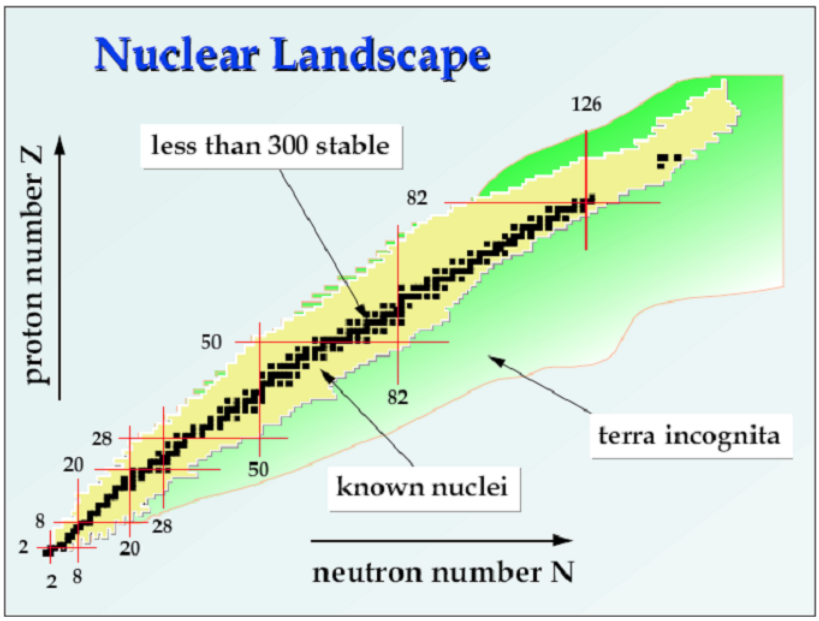

FIG. 1.3. Nuclear chart [3].

The neutron-rich region known as "terra incognita" is regarded as a final frontier in low-energy nuclear physics. In this region it is found that the nuclear shell model, which is regarded as the standard model of the nucleus, has been exposed as lacking quality in describing the nucleus. This model correctly predicts the location of shell gaps at the so-called magic numbers of protons and neutrons leading to very stable nuclei. However, some theoretical calculations and evidence from overseas radioactive beam facilities reveals a dissolution of the shell gaps in neutron-rich nuclei. This shows that with a RIBs facilities, we can be able to access information that is completely unknown [3].

Astrophysics

Nuclear astrophysics plays an essential role in understanding the structure and composition of the Universe and its constituents. The energy of stars is generated through nuclear reactions between stable as well as radioactive nuclei. One of the burning cycles, the so-called CNO (carbon-nitrogen-oxygen) cycle, has been suggested as an example of how intense radioactive-ion beams can be used to measure directly some properties of the key reactions at the relevant stellar energies [2, 4].

Materials Science

Radioactive-ion beams can be used as a superior diagnostic tool to provide detailed information on the environment into which the ions are implanted. Different methods have been developed over the years, such as the use of radio-tracers for diffusion studies in different materials, which relies on measuring the amount of radiation as a function of specific parameters.

A second way is through the hyperfine interaction between the atomic nucleus and its electron cloud, where studies of the interaction can lead to nuclear physics properties such as electromagnetic nuclear moments and, where nuclear properties are known, one can deduce information for the material such as the electric field gradient and hyperfine field [2].

Nuclear Medicine

Since the early days of nuclear physics, it was realized that nuclear radiation could be used in medicine for diagnosis and therapy. Medical radioisotopes today serve this double purpose [2].

1.4 Isotope-Separation-On-line Method

The separated-sector cyclotron (SSC) accelerator at iThemba LABS is part of the multi-disciplinary facility that supports research in nuclear physics as well as material science, and also provides radiotherapy where proton and neutron therapy are performed using proton and neutron beams respectively. Furthermore it also provides hospitals in South Africa and abroad with radioisotopes for medical diagnostics. However the shared use of this facility has reach the point where further growth is restricted. To address this issue a radioactive-ion beam (RIB) facility was proposed to solve this problem. With this new facility, radioactive-ion beam will be produced using the Isotope-Separation On-Line (ISOL) method.

The ISOL method requires two accelerators, one to produce radioactive atoms at rest

and the other to accelerate these radioactive beam up to energies of interest (sometimes only a few keV). This technique consists of several different steps which are: production, thermalization, ionization, extraction, mass-separation, cooling, charge-state breeding and acceleration. These processes are governed by physical (e.g. production cross-section, decay-half life, ionization potential) and chemical (e.g., molecular formation probability, volatility) properties of the nuclei of interest, and the properties of the target material are also important [5]. The production technique in the ISOL system requires the following properties: high efficiency, high production rate, selectivity and rapidity. Since we are dealing with short-lived exotic nuclei, the transportation of radioactive beam from the production site to the experimental station needs to be very fast to minimize the losses from radioactive decay [5].

The ISOL method uses a light-ion beam with energies ranging from a few MeV/nucleon to $\sim$ 1GeV/nucleon. The driver beam impinges either directly onto a fixed target or a neutron converter and then through spallation, fragmentation, fusion-evaporation and fission reactions, a wide range of rare isotopes can be produced [6]. The efficiency of these methods by which these rare isotope are extracted strongly depends on the applied ionization method, the target material and its thickness. There are two methods applied in the ISOL system, either a thick target, or a thin target with a gas cell coupled to an ionizer device. In both methods, a mass separator is used after the extraction of the ion beam, and the beam may be then delivered to an experimental station at low energy ($\sim$ 30 to 60 KeV) with a relatively low emittance beam [4].

Thick target ISOL

With this method, intense radioactive isotopes that lie far from the line of stability can be produced. However, this method cannot be described as a universal production technique since the efficiency can differ significantly due to the physical and chemical properties of a specific element [6]. The targets have thickness of few 100 g.cm^{-2} and consist of foils (e.g. tantalum), fibres, liquids (e.g. mercury) or powders (e.g. uranium carbide). The temperature at which the assembly is held depends on the specific physical and chemical properties of the investigated element. The target temperature may be kept almost at room temperature for production of noble gases and approximately 2000 K for production

of less volatile elements. The method employed to ionize the radioactive atoms is critically important for laser spectroscopy, since this will determine the velocity spread and beam properties [6].

Gas catcher and ion guide

In this method a thin target is placed into a gas cell. The nuclear reaction products recoil into a noble gas (Ar or He) where they thermalize and through charge exchange are left as neutral atoms or in a low charge state. This process is very fast and has a much lower chemical sensitivity compared to the thick target ISOL [6]. Ions are ejected from the gas cell through a small aperture in a high-speed gas jet into a differential pumping region where the ions are guided to a mass separator. The rapid thermalization time within the gas cell and subsequent extraction opens up the possibility of studying nuclear states with lifetimes below 1 ms. Different gas cells and ion guides have been developed, some including laser ion source techniques for selective ionization and extraction.

1.4.1 Advantage of ISOL

The advantage of the ISOL method is that it can operate on different target materials, which can be thick or thin. It can produce intense secondary beams and the beams have high purity which is element-dependent [7]. Also the beam quality is excellent with low emittance and energy spread. The ISOL method is capable of producing very intense beams at energies of interest to nuclear physics [7].

1.4.2 Disadvantage of ISOL

The main disadvantage of the ISOL method is that the yield is strongly dependent on the target or production chemistry and there is also a large amount of unwanted radioactivity from the reactions, which must be minimized [7]. The ISOL method is also affected by the delay due to diffusion or desorption (which is element-dependent) and the the time needed for preparation of the beam for the second accelerator (charge breeding, etc.).

1.5 Ionization Mechanisms

The ionization efficiency of an ion source is defined for a specific isotope as the ratio of the number of ions extracted from the ion source to the number of atoms injected into the ion source [5]. Different ionization mechanisms which have been implemented in ion sources of ISOL systems show distinct efficiencies. Any ionization mechanism that is applied in an ISOL system strongly depends on its application, e.g. ionization potential, required charge state and selectivity of the element of interest. A brief overview of the ionization techniques are given in the following sections.

1.5.1 Surface Ionization

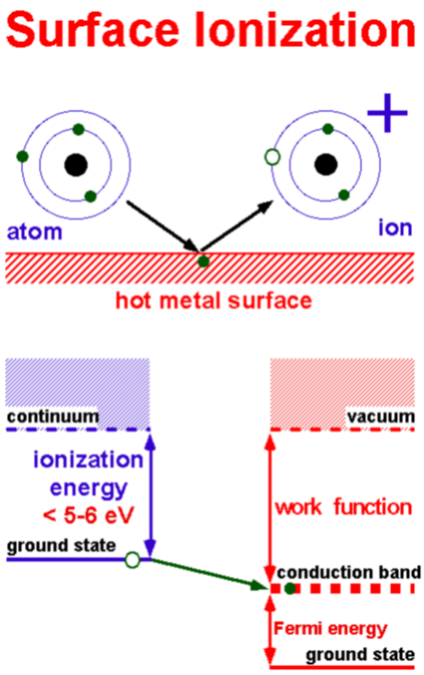

FIG. 1.4. Schematic representation of surface ionization [8].

In this mechanism, atoms interact with a hot surface so that they can lose or gain an electron before leaving the surface as positive or a negatively charged ions, and this creation of ions is referred to as positive and negative surface ionization, respectively [5]. This method is very efficient for elements with an ionization potential smaller than the work

function of the hot ionizer (noble metal surface), and it can also be used efficiently for elements with low ionization potential (less than 7 eV) for creation of positively charged ions and with electron affinity greater than 1.5 eV for creation of negatively charged ions. The heavier alkaline earths and the heavier boron group elements benefit from surface ionization due to their low ionization potential, but with reduced efficiency. The efficiency of this method strongly depends on the temperature of the ionizer material and the difference between the work function of the surface material (ionizer) and the ionization potential or the electron affinity of the element of interest [5, 8]. Figure 1.4 illustrates the principle of this mechanism [8].

1.5.2 Electron Impact Ionization

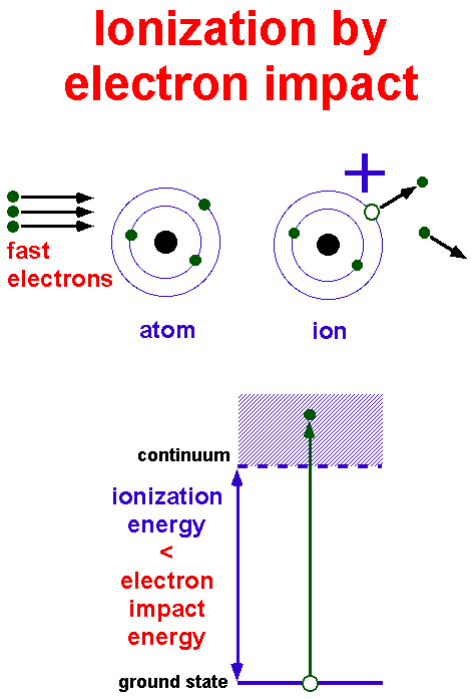

FIG. 1.5. Schematic representation of electron-impact ionization [8].

Here the atoms or ions are bombarded by highly energetic electrons, thereby losing one or more of their outer electrons [5]. This method is very efficient for elements with ionization potential greater than 7eV and for the creation of multiple charged ions. Figure 1.5 [8] illustrate the electron impact mechanism. The disadvantage of this mechanism is that it

is not selective.

1.5.3 Laser Ionization

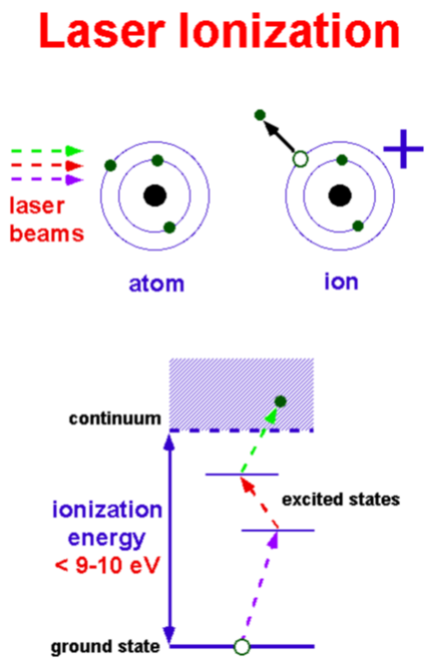

FIG. 1.6. Schematic representation of laser ionization [8].

In this process atoms are stepwise excited by laser photons, leading finally to the continuum, to auto-ionizing states or to highly excited states close to the continuum as shown in figure 1.6 [8]. To achieve maximum ionization efficiency, intense laser beams are used for excitation and ionization. The laser beams need to have a sufficient overlap in time and space with the atomic beam.

The first two mechanisms mentioned above do not show selectivity, which may result in a contaminated radioactive ion beam, which is contrary to our goal. The nature of resonant laser ionization makes this method more chemically selective because it consists typically of two or three (or even more) ionization steps which result in isobarically and isomerically pure radioactive beams of atoms [5]. For example at TRIUMF, J.P. Lavoie, P. Bricaulta, J. Lassena, and M.R. Pearsona calculated that the efficiency of producing radioactive beams

of ^{26}Al is better when laser ionization is used instead of surface ionization, i.e. 13% and 0.6% respectively [9].

1.6 Outline of the Thesis

The work reported in this dissertation aims to develop laser ionization using tunable dye lasers on a test-bench, in order to establish laser-ionization techniques for a planned radioactive-ion beam facility at iThemba LABS. We aim to acquire knowledge which can be used to develop the laser ion source for the production of RIBs using the existing beam from the SSC and a proposed demonstrator (see figure 1.7), where the existing beam from the SSC runs into the vault labelled N. The grey squares represent blocks of concrete while light grey represents hand-stacked concrete bricks for radiation shielding or protection. The beam from the SSC will be directed into the N vault, where it will hit the target (e.g. UC_x) and a laser ion source will be located for selection of rare, short-lived isotopes. The selected isotopes will be transported to experimental stations via the beam line with two analysing magnets as shown in figure 1.7. A laser ion source (LIS) is essential if radioactive-ion beams are produced via fission reactions, due to its high chemical selectively and high efficiency which can result in providing pure beams of single isotopes.

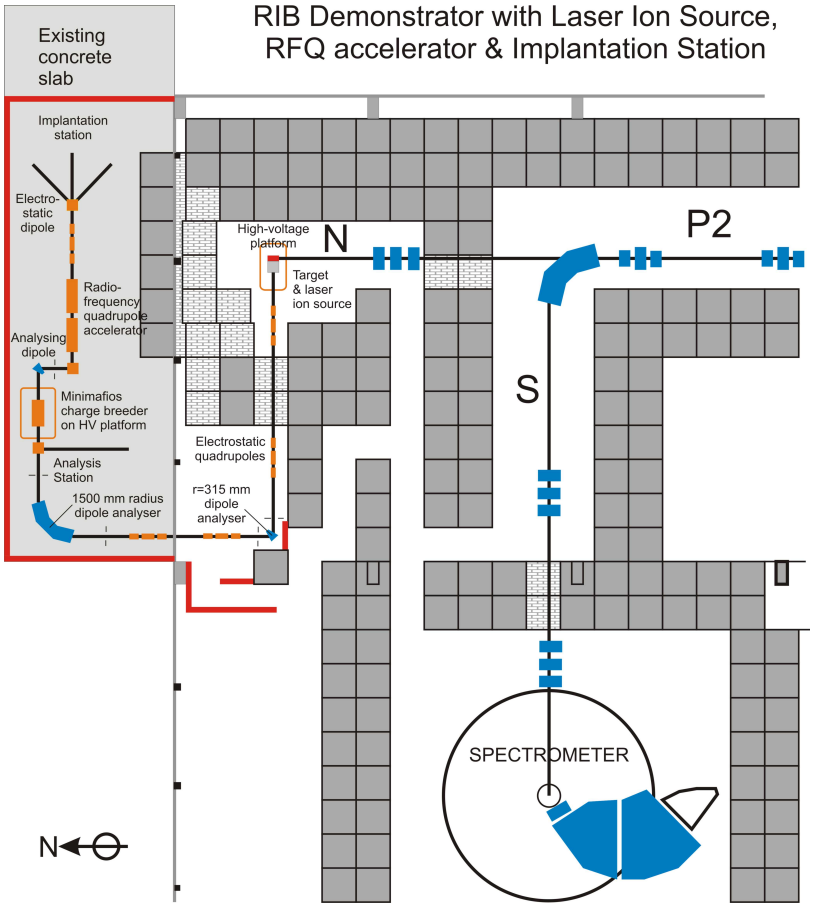

FIG. 1.7. iThemba LABS RIB demonstrator with laser ion source.

This technique of selective laser ionization of RIBs will be developed using stable beam of atoms (because the radioactive beams are not presently available). The technique will allow one to selectively ionize any element of interest extracted from a nuclear reaction (e.g fission reaction). Laser ionization is used in ISOL method for production of radioactive-ion beams. To achieve this process, step-wise excitation or ionization of atoms by laser photons is used because it provides a high level of selectivity and efficiency, as the unique electronic structure of different atomic species allows this technique to have chemical selectivity. In developing this technique, we use tunable dye lasers because they make it possible to match the photon energy of the laser to the electronic transition of the desired atomic species.

Chapter 2

Literature Review

2.1 Laser-Atom Interaction

Atoms have limited number of energy levels which are discrete in nature. When laser light (photons) interacts with the atom, the outermost (valence) electron in some initial state absorbs a photon and makes a quantum transition to a higher energy level provided that the energy of the absorbed photon is equal the energy difference between the two states involved:

$$E_f - E_i = h\nu \tag{2.1}$$

where ν is the frequency of the absorbed photon. Similarly, when an electron makes a quantum transition from the higher state to the lower state, it emits radiation (a photon) with energy corresponding to the difference between the two energy levels. The absorption and emission of photons in an atomic system is shown is figure 2.1.

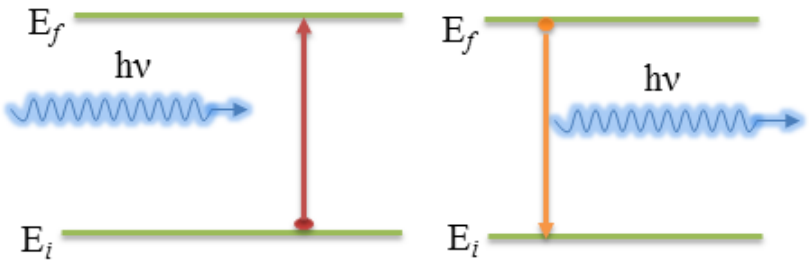

(a) Absorption (b) Emission

FIG. 2.1. Interaction of laser light with atoms

Laser light can be absorbed by any atomic or molecular system through many different processes such as multi-step and multi-photon absorption. These processes open new research fields due to properties of laser light such as monochromaticity, directionality, coherency and high intensity.

2.1.1 Multiple-step and multiple-photon excitation or ionization

Resonance multi-step ionization was implemented for the first time during 1980's [10], and since then and until the present time, various modifications of schemes for multi-step and multi-photon ionization method have been developed in the laboratory for solving numerous problems such as detection of extremely rare isotopes and single atoms, detection of short-lived nuclei in accelerators, separation of isotopes, nuclear isobars, and nuclear isomers. In multi-step photon absorption, an atom can successively absorb photons of different wavelengths, depending upon the lifetimes of the intermediate levels [11, 12]. The simplest example is the two-step photon absorption which is described below.

All possible resonance ionization schemes can be classified by several characteristic features such as the number of independent wavelengths used, number of excitation stages, including both resonant and non-resonant transitions, the type of multi-photon resonance and non-resonance used and total number of the absorbed photons [10]. In principle, the resonance ionization of any atom can be effected by the two-step excitation scheme and all two-step schemes can be divided into four types as indicated in figure 2.2.

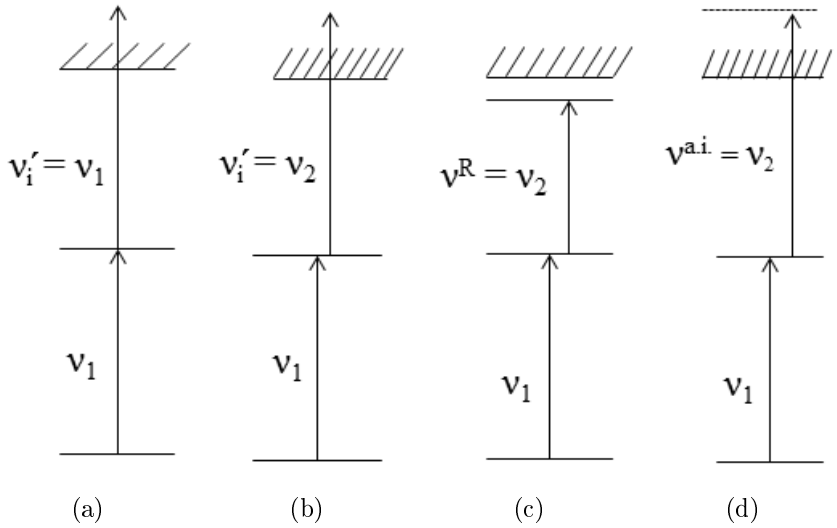

FIG. 2.2. Various types of two-step excitation, where $\nu^{'}$ means that the second step is non-resonant.

In figure 2.2 $\nu^{'}$ indicates the absorption of a photon in a non-resonant excitation stage resulting in a direct transition to the continuum. The various two-step excitations in figure 2.2 can be classified as follows, where A will represent an atom in its ground state while A^* and A^{++} will represent excited atoms using different wavelengths: In (a) the ionization is in the single-frequency field ν_1 with only one excitation stage being in resonance

$$A(\nu_1, \nu_1^{'}) \rightarrow A^* \tag{2.2}$$

In(b) two different wavelengths are used to ionize with only one wavelength being in resonance.

$$A(\nu_1, \nu_2^{'}) \rightarrow A^* \tag{2.3}$$

In (c) and (d) the ionization is in a two-frequency field (different wavelengths) and the excitation stage are both in resonance.

$$A(\nu_1, \nu_2^{R}) \rightarrow A^{++} \tag{2.4}$$

$$A(\nu_1, \nu_2^{a.i.}) \rightarrow A^* \tag{2.5}$$

Resonant absorption of the second photon frequency ν^R and $\nu^{a.i}$ represents the transition to a higher excited known as Rydberg states (a state close to the continuum where atoms

can be either ionized by electric field or collisions) and to an auto-ionizing (a process whereby atoms spontaneously lose one of their valence electrons to become ionized) state respectively. The higher excited state (A^{++}) can be ionized either by an electric field or by collision [10]. In any of the excitation methods mentioned above, selection of the excitation transition has an important effect on the ionization efficiency.

The benefit of the multiple excitation and selectivity is that it provides the maximum probability of exciting the atoms to the high-lying state. The disadvantage of multiple steps is that this requires as many lasers as the number of the steps that have to be accessed to reach the final excited state. In most cases multiple excitation is employed because it does not suffer from limitations such as poor transition probability and leaving atoms in excited states that lie too far below the continuum. Selection of the excitation transition (wavelength) has an important effect on the ionization efficiency (and the sensitivity of the signal obtained).

2.2 Resonant Laser Ionization

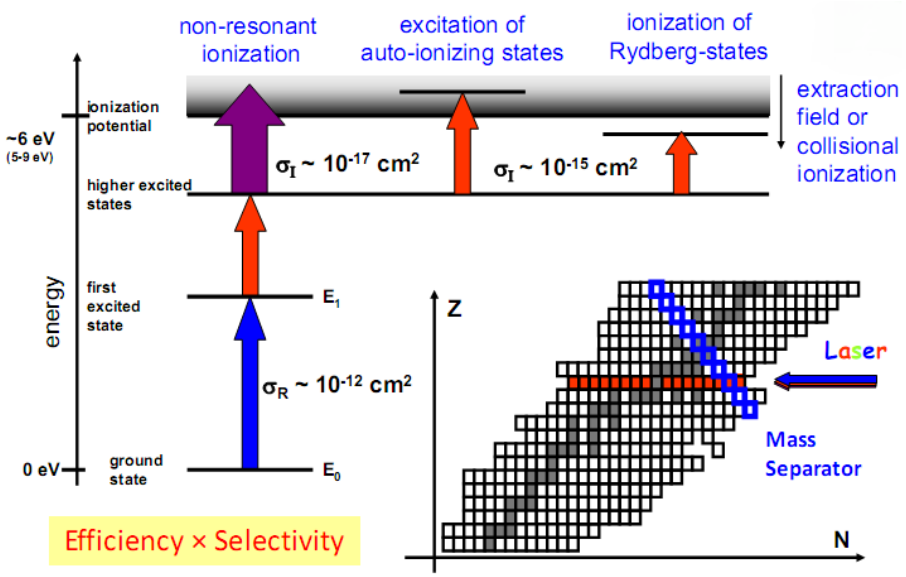

FIG. 2.3. Principle of resonant laser ionization and possible ionization scheme where σ is the ionization cross section, and isotope selection by combination of RILIS and mass separation[13].

Resonant laser ionization (RLI) refers to the creation of an ion from a neutral atom when it is resonantly excited and ionized by a laser photon [14]. Resonant laser ionization can be achieved by using tunable lasers because it is possible to match the photon energy of the laser to the electronic transition of the desired atomic species and gives this method a better selectivity. Mostly multiple-step ionization is used because it is more selective than the single step which suffers from the limitation such as stimulated emission, and using strong intense beam can cause it to depopulate other states. The development of resonant laser ionization led to a new source for producing radioactive-ion beams called a resonant ionization laser ion source (RILIS). Figure 2.3 shows the basic principle of resonant laser ionization with typical cross sections; this also shows that atoms can be excited into different atomic states in order to be ionized, i.e. ionization of Rydberg states, excitation of auto-ionization states and non-resonant ionization. These processes have different cross sections.

2.2.1 RILIS

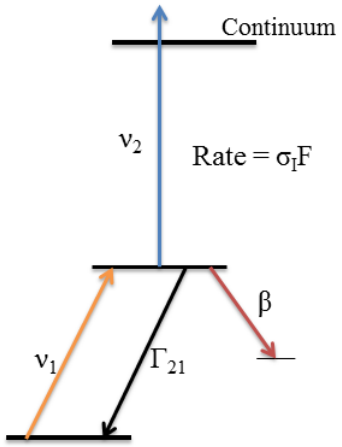

FIG. 2.4. Schematic diagram representing the atomic level scheme of resonant ionization. The rate of ionization is σ_IF where σ_I is the ionization cross section, F is the flux of photons, Γ_{21} is the natural radioactive decay and β is the loss rate from the metastable state [15].

High selectivity can be obtained using several intermediate steps, and RILIS is used in order to obtain ion beams of high intensity and high purity. In figure 2.4 we show an idealized two-step ionization scheme. The conditions needed for 100% ionisation of the

atoms irradiated by the laser can be deduced from the rate equations for the population of the different atomic levels [5]. This leads to a condition on the flux (the number of photons per unit area per second) and on the fluence (the number of photons during the laser pulse per unit area) of the laser photons. Since the cross section for the first excitation step is larger, the ground and excited state are in equilibrium during laser irradiation. Under this condition the number of excited atoms ($N(t)$) can be obtained from

$$-\frac{dN(t)}{dt} = (\sigma_I F + \beta)N(t) \tag{2.6}$$

where σ_I is the cross section for ionization from the excited state to the continuum: the probability of photo-ionization of an atom is proportional to the photo-ionization cross section of the atom to its ionic state, $F(\text{in cm}^{-2}\text{s}^{-1})$ is the flux of photons, and β the depopulation rate of the excited state due to natural decay or other loss mechanisms. It is assumed that the laser pulse fires at $t = 0$ and then from equation (2.6), conditions on the flux and on the fluence of the laser photons are obtained. The flux condition requires that the depopulation rate of the excited state by ionization into the continuum is much larger than that of the natural decay.

$$\sigma_I F \gg \beta \tag{2.7}$$

The fluence condition requires that in total (i.e. in one laser pulse) sufficient photons are used to irradiate the atom to induce the ionization step, i.e.

$$\sigma_I \phi \gg 1 \tag{2.8}$$

where ϕ (cm^{-2}) is the fluence. If both equations (2.7) and (2.8) are fulfilled this means that complete saturation is reached, i.e. basically all the atoms irradiated by the laser light are ionized [5].

2.2.2 Laser ion source

The operational principle of the ion source is based on the selective laser resonant ionization of nuclear reaction products either emitted into a vacuum or stopped in a high-pressure noble gas [16, 17]. These radioactive species defuse out of the target catcher system where they are stored for a certain period in a heated cavity preventing them from sticking on the walls of the chamber. The average time these atoms spend in the hot cavity ranges from 10 to 100 μs: therefore to assure that each atom interacts with the laser light, laser systems with repetition rates of the order 10 kHz are used [8, 15]. This ion source is almost identical to the ionizer tube of a surface ion source but elements with low work function such as Ta, Nb or W are used to prevent surface ionization. Due to the development of this ion source, materials such as ceramics or with ever lower work functions have been suggested to cover the inside of the cavity [14, 15]. As shown in figure 2.5, the radioactive species produced are irradiated several times by the laser beam before leaving the cavity. Figure 2.6 shows the SPES target design where a proton beam hits a UC_x target and the reaction products recoil out.

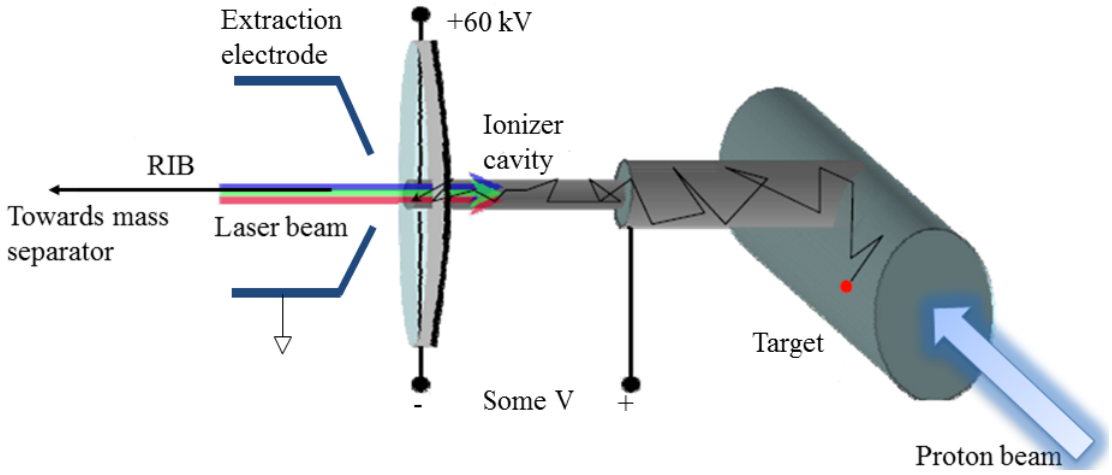

FIG. 2.5. Schematic diagram of laser ion source [18].

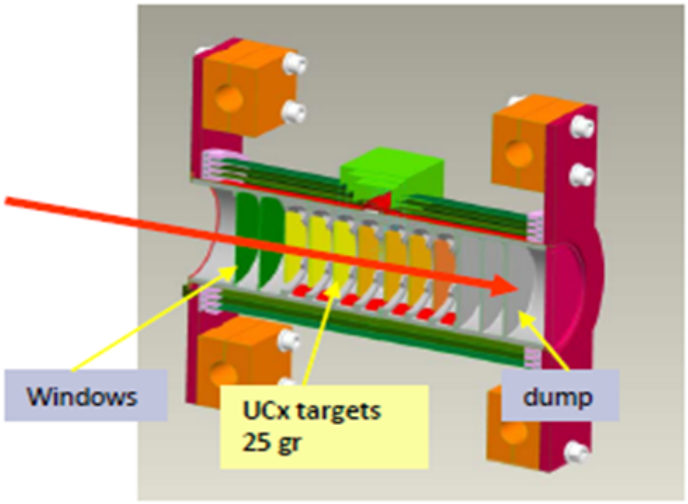

FIG. 2.6. Conceptual target design [19].

Some conditions have to be fulfilled in the construction of the laser ion source e.g. the reaction products recoiling out of the target have to be stopped in a hot cavity. The efficiency depends on the number of the measured ions and the number of ion produced in the target. The selectivity of this ion source is given by the ratio of the ion current when the lasers are tuned on resonance and off resonance. The temperature of the cavity also plays a role in determining selectivity [15]. At ISOLDE they successfully use this type of laser ion source for different measurements related to exotic nuclei [14].

2.3 Photo-ionization cross section

The photo-ionization cross sections of many atoms in the ground state are well known, while for higher excited states little information is available. Cross sections are usually higher near the ionization threshold and decrease with an increase in photon energy. Different methods (i.e. theoretical and experimental) have been developed to measure and estimate the photo-ionization cross sections.

Theoretical techniques that have been developed to calculate photo-ionization cross sections are: the Many-Body Perturbation Theory (MBPT) method, Close-Coupling (CC) method, R-Matrix method, Random Phase Approximation (RPA) method, Relativistic method, Transitional method and Multi-Configuration Hartree-Fock (MCHF) method [20].

These methods have successfully calculated the photo-ionization cross sections of different sub-shells of atoms. Photo-ionization cross sections can be deduced from experimental techniques such as the saturation method. The saturation condition requires 100% probability of excitation of all atoms in the laser ionization region in a time shorter than the life-time of the level being excited:

$$\sigma \tau I > 1 \tag{2.9}$$

where τ is the life-time of the excited level, σ is the excitation cross section and I is the incident photon flux. This condition of saturation can be used to find the minimum laser radiation required to saturate a transition, i.e. typically, for atomic levels with life-times from 10^{-8} to 10^{-6} sec, the radiation power needed for resonant excitation ranges around 1 W/cm^2 and for non-resonant transitions it is around 10^8 W/cm^2 [21]. The saturation condition for the laser pulse is:

$$\sigma I \Delta t > 1 \tag{2.10}$$

where Δt is the pulse duration and I is the laser pulse radiation intensity. The probability that a photon of a given energy can be absorbed by an atom to excite the photoelectrons is given by

$$\sigma(h\nu) = \frac{P(h\nu)}{I(h\nu)} \quad \text{(barn)} \tag{2.11}$$

where P is the number of photons absorbed per unit time and I is the incident photon flux, defined as the number of photons per unit area per second.

2.4 Result obtained from previous studies using RLI

Figure 2.7 shows some of the elements in the periodic table that have been studied using the RILIS method. Different ionization schemes have been developed for each atom.

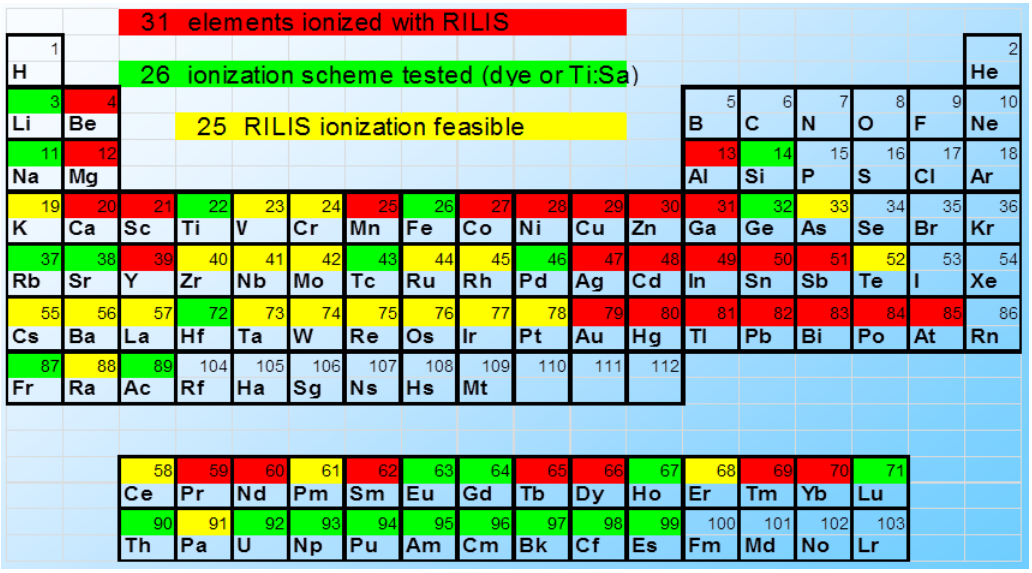

FIG. 2.7. Element ionized by different RILIS mechanism [8].

Chapter 3

Laser-Enhanced Ionization in air

3.1 Introduction

In this section we discuss laser-enhanced ionization (LEI) and some of the equipment used. Selective ionization of strontium will be performed in a gas and the current will be measured to demonstrate ionization. We will conclude by discussing the result obtained using this method.

3.2 Principle of Laser-Enhanced Ionization

The laser-enhanced ionization principle is characterized as the method in which enhancement of normal collisional ionization rates is obtained by optical excitation of atoms by resonant laser excitation [22]. The LEI technique utilizes selective laser excitation of atoms followed by collisional ionization or photo-ionization in flames, atomic beams and discharges [23]. A sample to be analysed is aspirated into a flame via a nebulizer and the sample vaporises to an aerosol and is then atomized (atomization is the process whereby the sample being analysed is converted to atomic vapour in order to make an interaction between the light and matter possible [24]). The atoms have to be selectively excited to states with higher ionization probability, then exposed to collisions in order to be ionized. The ions and electrons created have to be collected in order to contribute to the measured signal.

LEI spectroscopy is typically applied to atoms in flames, furnaces, cells and discharge lamps which are currently used by other optical spectroscopic techniques [22]. Flames are used because they provide high quality atomization and ionization of elements and good detection charges. The LEI signal appears as a change in current and the current is easily detected by using the pulsed or amplitude-modulated continuous-wave (cw) lasers with synchronous detection. Excitation of the atoms can be performed with either pulsed sources or continuous-wave sources. Even if there is no inherent disadvantage in using cw-laser light, most LEI is done with pulsed dye-laser systems. One advantage of pulsed dye-laser systems as compared to continuous-wave tunable laser systems is that pulsed light sources are able to produce light of much higher intensity than that from cw sources, especially in the UV region [25]. In LEI the ionization is thermal in nature and detection sensitivity depends strongly on the proximity of the excited level to the ionization threshold i.e. the excitation scheme chosen for the given element.

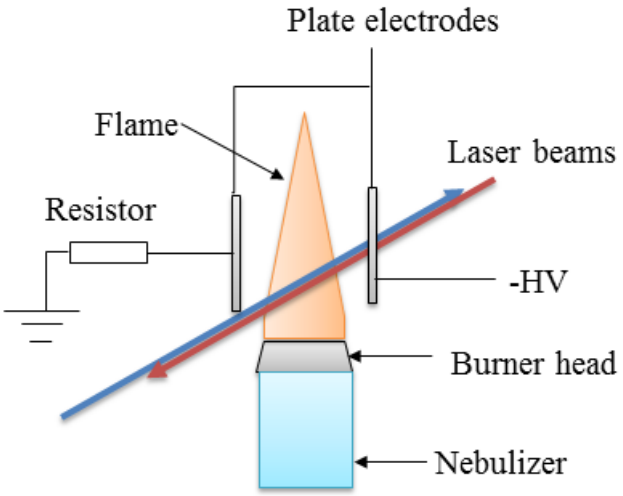

FIG. 3.1. LEI.

The maximum current density that can be obtained (extracted) from a flame by applying an electric field is a measure of the volume ionization rate of the flame [26]. An external field is applied to sense the current change resulting from the laser-atom interaction and collisions as shown in figure 3.1. The charges created are directed by the electric field and they travel at finite velocities (much less than the speed of light). Different types of electrodes such as flat plates may be used as horizontal electrodes, i.e. as an anode and a cathode [27]. The electric field is directed perpendicular to the electrodes, imparting

a horizontal velocity to the electrons in the direction of the anode and pulling positive ions toward the cathode. Positive or negative high voltage is applied to one plate while the other one is grounded through a load resistor. At high voltage, ions and electrons are centred approximately at the same height above the burner head below the laser atom interaction, while at low voltage, ions and electrons are distorted above the burner head resulting in broadening of the spectrum.

The ionization yield refers to the fraction of illuminated atoms that are ionized as a consequence of laser irradiation [28], and it is a measure of both the laser excitation efficiency and the collisional processes. Collisional ionization is of primary importance in determining the ionization yield because it directly determines the sensitivity of analytical laser ionization spectrometry techniques. Ionization efficiency is defined as the probability that an excited atom will ionize before returning to the ground state.

The limit of detection (LoD) in LEI for signal collection can be high for the following reasons: the incomplete atomization of analyte species in the flame, high contamination levels from the blank solutions (solution of known concentration used to calibrate the instrument) and poor choice of excitation wavelength leading to spectral interference or excitation levels lying too far below the ionization threshold. The use of electrodes for signal collection makes LEI vulnerable to the presence of easily ionizable elements in the sample [29]. The charge created by the thermal ionization of easily ionizable elements tends to increase the signal-to-background noise, depressing the electric field gradient between the electrons and reducing the LoD [22]. The LoD of atoms is limited by the following factors, namely fluctuations of the background current between the electrodes that detect the signal, non-selective ionization of atoms and molecules in the flame and ionization noise of the input resistance of the signal pre-amplifier.

3.3 Laser system

The laser system used consisted of two dye lasers pumped by an excimer laser. The two dye-lasers operate with different organic dyes and the excimer laser operates with xenon-chloride (XeCl). A brief description of both types of lasers is given below.

3.3.1 Tunable Dye-Laser

3.3.1.1 Excitation of dye molecule

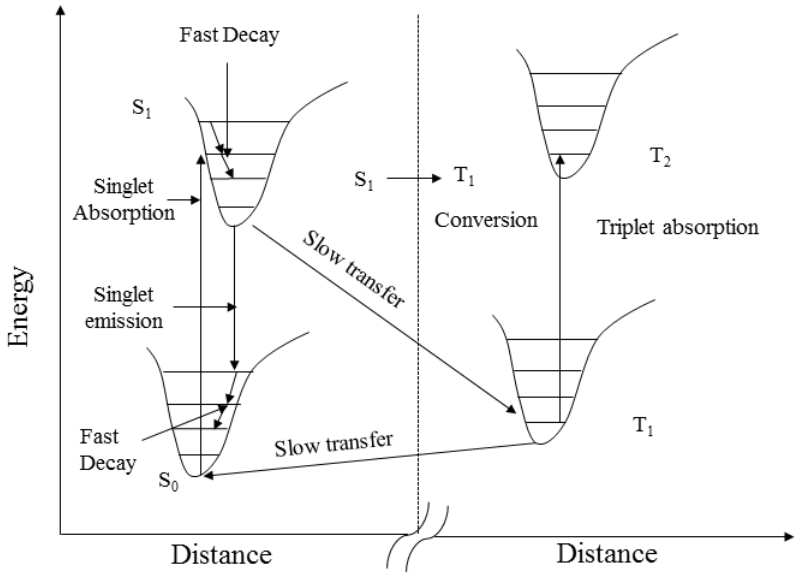

FIG. 3.2. Typical energy level diagram of a dye molecule [30].

The active molecules in this laser are large organic molecules dissolved in a pure solvent such as methanol. The most magnificent feature of dyes is their tunability. Figure 3.2 shows the typical energy level diagram of dye molecules with electronic levels associated with vibrational and rotational energy levels. The symbols S_0, S_1, T_1 and T_2 represent the energy levels associated with manifold vibration and rotational energy levels. S stands for singlets while T stands for triplets. The total electronic spin quantum number for a singlet state is S=0 while for a triplet is S=1. A level can have a total degeneracy of 2S+1. The names singlet and triplet refer to the number of possible magnetic substates (1 and 3 respectively). The transition from S↔S and T↔T are allowed while transitions from S↔T are forbidden due to the section rule which says that any transition that results in electronic spin change ΔS=1 is forbidden [30, 31].

As it is shown in figure 3.2, S_0 is the singlet state, so practically all the dye molecules are in the S_0 level, hence the population within this state is described according to the Boltzmann distribution law, that at room temperature most of the population within the ground state is at the bottom of the state. Because of the forbidden transition (S↔T),

optical pumping can excite the molecules to higher energy singlet states (S_1, S_2, etc.) The transition $S_0 \rightarrow S_1$ is possible over broad frequency region because S_0 and S_1 are associated with a broad range of vibration-rotation states. The transition frequencies probably lie in the near-visible or visible range so that the dye has the particular colour due to selective absorption, and owing to the large size of these organic dye molecules, their oscillation strength for the allowed transition is also large [30, 31]. Dye lasers are tunable because the transition $S_1 \rightarrow S_0$ also ends in a broad range of final states.

3.3.1.2 Basic Description

Dye-lasers are special types of lasers that produce light in a liquid lasing medium. They are given this name because dyes are organic compounds that contain conjugate double bonds and the presence of double bonds make these compounds optically active (fluorescent). These strongly emitting and absorbing dyes are dissolved in a suitable polar solvent like ethanol or a nonpolar solvent like chloroform at 10^{-4} to 10^{-3} molar solution to serve as a lasing medium [30]. They cover the spectral range from 320 nm up to 1200 nm and the tuning of each dye can be 40-60 nm. When they are used sequentially, continuous tunable laser action can be active from near-UV to the IR region and the extended frequencies at both the shorter and longer wavelengths are produced by sum and difference frequency mixing [30]. These dye-lasers are pumped by different high-power lasers (such as excimer, Cu vapour or nitrogen lasers) to produce an output power of up to 25 W and output energy up to 100 mJ or more over a duration of the order of 10 ns. Also, the output pulses can be up to tens of millijoules in a 10 ns pulse in a beam of a few millimetres in diameter at repetition rates of up to 1 kHz [30].

Inclusion of a wavelength-selective element inside the resonator cavity enables the output wavelength of these lasers to be tuned. Diffraction gratings or prisms are used as wavelength selectors. The grating is superior in terms of large dispersion and wavelength resolving power. The use of a telescope lens increases the number of grooves illuminated by the laser light and reduces the light intensity on the grating, preventing the damage on the coating on the grating surface. The line width of the telescope-grating-cavity dye-laser is of the order of 0.1 nm; to further reduce the line width to the 0.01 nm to 0.05 nm range, an intra-cavity etalon is used [30].

3.3.1.3 Operation

The dye-laser is pumped by a beam which is split into several separate beams (as shown in figure 3.3), and one beam is used to pump a narrow-frequency output tunable oscillator containing a beam expander, and also a grating as explained in following.

Pump beam path

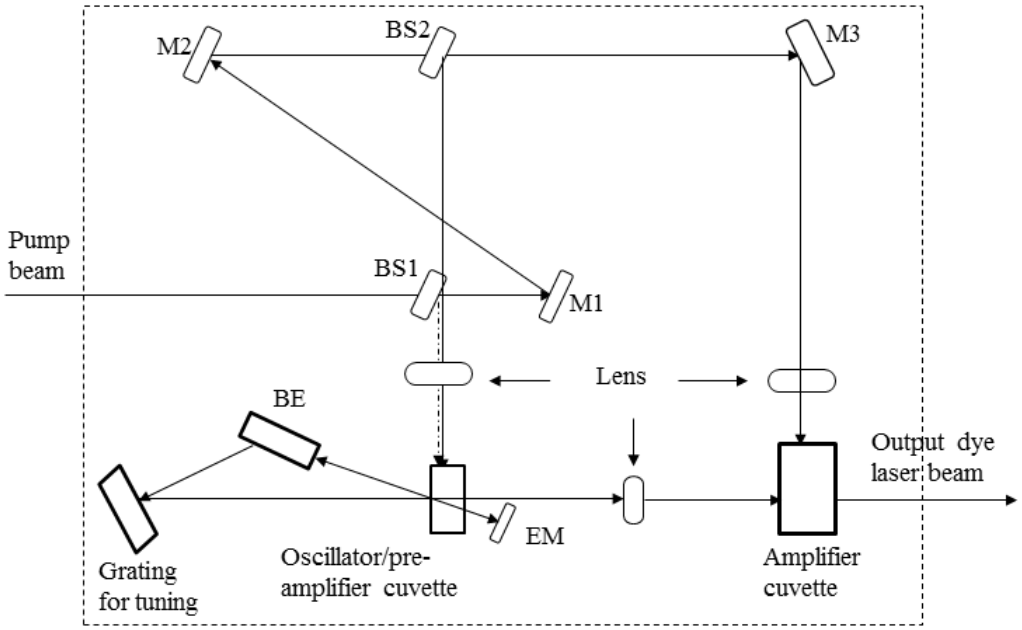

FIG. 3.3. Dye laser oscillation, where M represents a mirror, EM represents an end mirror while BS and BE represent the beam splitter and beam expander respectively. The oscillator/pre-amplifier cuvette and amplifier cuvette are filled with dye solutions of different concentrations.

The pump beam goes through the oscillator beam splitter (BS1) where 10% of the beam is split off and reflected towards the oscillator/pre-amplifier dye-flow cuvette. Then the remaining pump beam hits mirror 1 (M1)where the pump beam is raised by 25 mm to fall onto mirror 2 (M2). This mirror (M2) reflects the beam to run parallel with the pump beam. When the pump beam crosses the pre-amplifier beam splitter (BS2), 10% of the pump beam is split off and reflected towards the oscillator/pre-amplifier cuvette. The delay between the pump beam for the oscillator and the pump beam for the main amplifier is 4 ns. Lastly, the pump beam hits mirror 3 (M3) and is completely deflected by 90° towards

the main amplifier. The oscillator and pre-amplifier pump beams are focused into the oscillator/pre-amplifier cuvette by cylindrical focusing lenses.

Oscillation and pre-amplification

The oscillator of the dye laser consists of the dye-flow cell and pump optics, tuning block and the cavity end mirror. The tuning block contains all components that determine the wavelength of the oscillator radiation. The grating (with grating constant of K = 600 grooves/mm, 2.7 micron blaze, Zero-Dur substrate) can be tilted between Littrow angles of 42.5° and 72.5°. The grating is mounted on a precision sine drive for wavelength linear tuning. The end mirror is located at the right of the oscillator/pre-amplifier cuvette crate. The first part of the oscillator beam path runs between the cavity end mirror, through the oscillator/pre-amplifier cuvette and into the prism beam expander. Inside the beam expander the beam is expanded vertically. The expanded beam then leaves the expander as a light ribbon falling onto a grating perpendicular to the grooves (diffraction channels). For a beam path with wavelength matching the Littrow condition $\lambda_0 = 2sin\alpha$/K.N (where N is the order of the grating used), light is reflected back, following the incoming path throught the beam expander and the pump region on the end mirror. To tune the wavelength, $sin\alpha$ is changed by rotating the lead screw of the sine drive. The output beam of the oscillator is derived from the reflection of the oscillator beam at the entrance prism where 25% of the oscillator beam is split off and routed to the grating, hitting it at the point of rotation, where it reflected at 4° back into the oscillator pre-amplifier dye cuvette. For further details of the grating and better understanding of dye laser equipment and oscillation in a resonator cavity, **experiment A.1** described in **appendix A** was conducted.

Main amplifier and final adjustment

The flow cuvette of the main amplifier is approximately 40 mm wide with 2.5 mm gap between the pump window and the metal flow guide inside the cuvette. The cell is inserted once it is filled with dye solution and the dye solutions are typically in the ratio of 1:3 in the respective cuvette cells i.e. the amplifier is filled with solution that is diluted three times more than that of the oscillator/pre-amplifier. To get experience in designing and aligning the laser beam, **experiment A.2** was conducted (**see appendix A**).

3.3.2 Excimer Laser

The term 'excimer' is a contraction of the phrase 'excited dimer' which is a molecule that only exists in excited states because its ground state has a very short half-life, resulting in a repulsive force between the two atoms of the molecule [24]. Since these molecules do not exist in the ground state, indirect pumping is used (such as electron-beam pumping, pumping by an electrical high-pressure gas discharge or by microwave) to reach the required energy. These excimer molecules are gases which contain a halogen and a noble gas, and are highly corrosive. Excimer lasers have an important feature, which is that they cover a wide range of wavelengths (i.e. from visible to the ultraviolet region) depending on the excimer employed [31].

Excimer laser wavelengths are produced by forming the excited state of the species of the excimer molecule in the upper laser level. When an electric discharge or electron beam is initiated within the lasing medium, then the noble gas atoms are excited and ionized (Y^* and Y^+) and the halogen molecules (i.e. X_2) dissociate to produce halogen atoms (i.e. X) [31]. Many of the halogen atoms (X) rapidly collect the free electrons (produced by ionizing Y) to form X^- negative ions. (e.g. X = Xe, Y = Cl). The ion-ion recombination process then occurs in which ions X^+ and Y^- combine to form an excited XY^* molecule (e.g. $XeCl^*$)

$$X^- + Y^+ \rightarrow XY^* \tag{3.1}$$

The $XeCl^*$ molecule emits radiation, leaving the molecule in the ground state which immediately dissociates to producing Xe and Cl atoms. The process starts again when the next pulse of the electron beam arrives.

3.4 Experimental setup

In this experiment we want to investigate laser ionization of strontium atoms in a solution to populate a specific energy level using tunable dye-lasers.

3.4.1 Experimental details

Charges created in LEI are collected by applying an electric field across a flame by means of an electrode arrangement and measuring the corresponding current between the electrodes [22]. Most familiar types of electrode arrangements used in a flame are shown in figure 3.4. The electrode designs used in most cases are displayed in figure 3.4 (a), (b) and (c), where the burner head is electrically isolated and acts as an electrode to measure the current signal. In most LEI setups, the electric field is established in the flame either by a flat electrode or rod, a split-cathode arrangement, or by an immersed electrode placed at the centre of the flame. It is also possible to apply an electric field horizontally across the flame by biasing two electrodes differently, as shown figure 3.4 (d). The split-cathode arrangement can be used for analytical purposes because of its stable electric field distribution, high contamination resistance and long life-time [22]. Immersed water-cooled electrodes can be used to reduce interference from thermal ionization of easily ionized species and these electrodes are usually placed in the centre of the flame. The water-immersed electrode used in this experiment to collect the charged particle created is shown in figure 3.4 [22] (c).

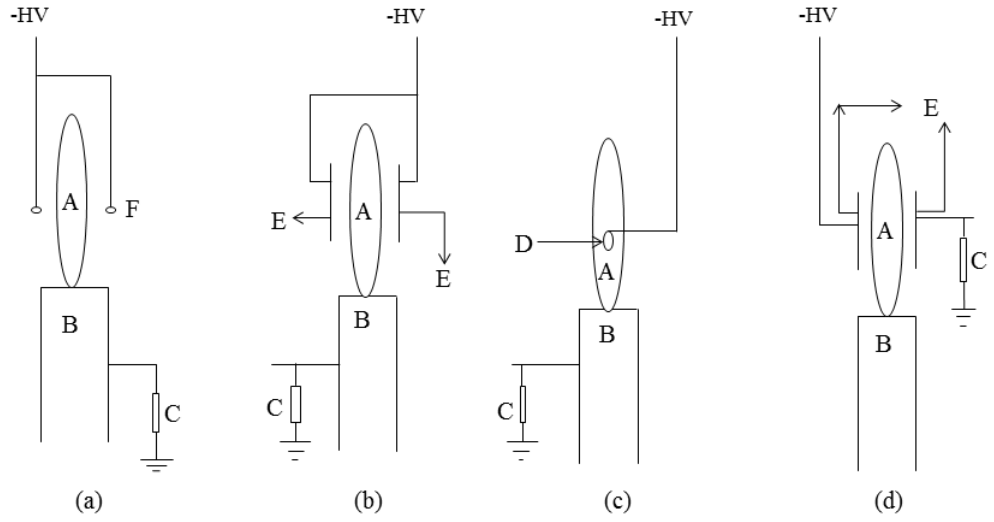

FIG. 3.4. Various schematic designs used in the LEI setup: (a) and (b) are designs for a split-cathode arrangement, (c) is the immersed water-cooled electrode and (d) is used for measurement at low voltage. The letters represent respectively: A a flame, B a burner head, C a resistor, D an immersed water-cooled electrode, E a plate electrode and F a rod electrode [22].

3.4.2 Excitation mechanism (single or multiple-step)

Several elements can be efficiently excited to higher excited states using a multiple-step excitation (e.g double- or triple-step) scheme, while in other cases single-step excitation can be used, but the problem is that the single-step suffers from limitations such as poor transition probability, which means they leave atoms in a state that lies too far below the ionization threshold. Depending on the mechanism employed, the selection of the excitation transition (wavelength) has an important effect on the ionization efficiency and the sensitivity of the observed signal. Figure 3.5 (a) and (b) demonstrate single- and two-step excitations followed by collisional ionization in the flame.

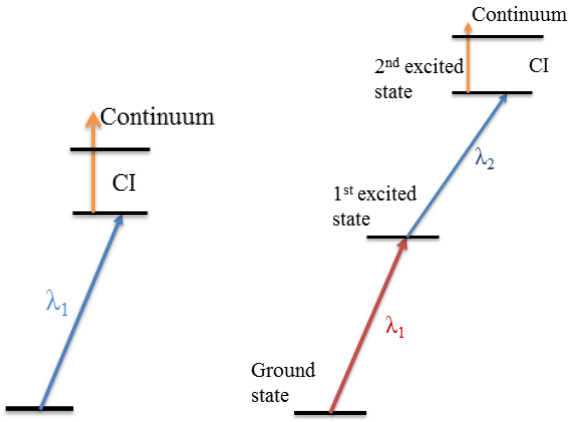

(a) Single Step (b) Two step

FIG. 3.5. Excitation mechanisms used in LEI where CI means collisional ionization.

Using too much laser power may also cause depopulation of the excited state via stimulated emission which may reduce the efficiency. The choice of laser is very important because of its influence on factors such as the number of states that can be populated. If the laser beam has too much power it may also populate other states causing the process to be non-resonant instead of resonant laser ionization.

3.4.3 Atomic population

The nature of the signal obtained depends on the type of the atomizer employed and the method applied to introduce the sample into the flame. The sample is introduced

continuously in the form of droplets via a nebulizer, converting the solution into a fine spray of droplets and this process is called nebulization [24].

The flames used in spectrochemical analysis are hot, highly exothermic, and an auto-catalytic chemical reaction takes place in the gas phase between the fuel (acetylene) and oxidant (oxygen). After the flame is ignited, it propagates through the combustible mixture. The flames are kept stationary by means of the burner which supplies the reaction gases and supports the combustion reaction. The oxidant and fuel are continuously supplied to the burner and ignited on the top of the burner head. We have two types of flames, i.e. premixed and un-premixed flames, in which fuel and oxidant are mixed prior to the region where combustion takes place, and in which oxidant and fuel are mixed in the combustion region itself, respectively [24].

The flame temperature is calculated based on the ideal adiabatic condition and thermodynamic equilibrium. Experimental temperature depends on the conditions used, such as the gas flow-rate, fuel-to-oxidant ratios, burner design, position in flame, and presence or absence of the liquid droplets. The use of oxygen instead of air increases the theoretical flame temperature, and acetylene flames are often achieved under fuel-rich conditions because the combustion products are partly dissociated. The reaction taking place in the acetylene is as follows

$$C_2H_2 + O_2 + 4N_2 \longrightarrow 2CO + H_2 + 4N_2 \tag{3.2}$$

and the stoichiometric temperature obtained from this reaction is 2540 K [24].

3.4.4 Experimental setup

The LEI experimental setup used is illustrated in figure 3.6 below

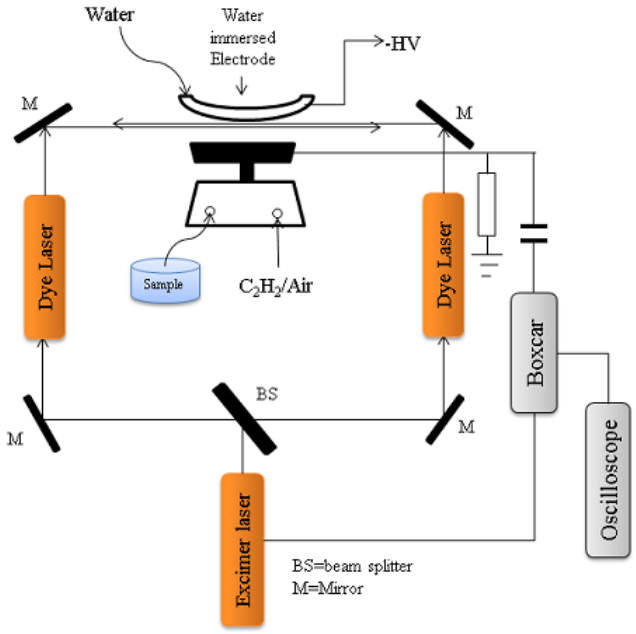

(a) Schematic diagram

(b) Photograph of the setup

FIG. 3.6. Laser-enhanced ionization experimental setup.

3.4.5 Experimental procedure

Two laser beams were used to excite strontium atoms in the following transition, where they overlapped temporally and spatially above the centre of the burner head.

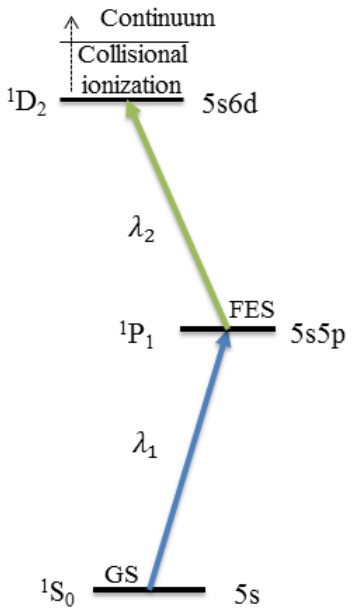

FIG. 3.7. Excitation wavelengths used for strontium, where $\lambda_1 = 460.79$ nm and $\lambda_2 = 554.331$ nm, while GS and FES means ground state and first excited state, respectively.

The LEI apparatus shown in figure 3.6 consists of the flame burner assembly and a water-cooled electrode to collect the charges created in the flame. To generate the atomic element in the flame, a burner head coupled with an interlocker system for gas control was used. The flame was fed with acetylene and air in approximate stoichiometric proportions. Two tunable dye-lasers (Lambda Physik, FL2002) were pumped by the excimer laser (Lambda Physik, LPX-240i) and the excimer laser was operating on XeCl at 308 nm. The dyes used were Coumarin 460 and Coumarin 540A dissolved in the pure solvent (methanol). The output wavelengths of the dye-laser could be tuned to the specific wavelength of an atomic transition and the wavelengths as shown in figure 3.7. The counter-propagating laser beams from the two dye-lasers were directed horizontally through the flame just grazing and just below the water-cooled negative electrode. The two lasers of different wavelengths were simultaneously directed into the flame and they were pumped simultaneously by the excimer laser.

The strontium concentrations used ranged from 10 ppm (μg/ml) to 1% (10000 ppm) produced from a commercial stock solution. The electrons created were collected by means of applying a negative high voltage (up to 1000 V) between the pairs of electrodes to measure the current (the measured signal). The influence of the electrode gap at constant

applied voltage as well as the influence of applied voltage at constant electrode gap were investigated.

3.5 Data acquisition

The current obtained was fed to the "boxcar" integrator (SR 250) for signal processing and the result was displayed on the digital oscilloscope TDS 1020. A boxcar integrator is a device for measuring repetitive signals, particularly those with short pulse duration and small duty cycles. It allows the recovery of signals that are time-related to a trigger signal and rejection of those that are not. The boxcar integrator (SR 250) consists of a gate generator, a fast gated integrator and exponential averaging circuitry. The SR 250 may be triggered internally or externally. The delays can be adjusted from nanoseconds up to milliseconds and the width can be adjusted from two nanoseconds up to fifteen microseconds.

3.6 Result and Discussion

Two dye-lasers were used to excite strontium atoms from the ground state to the first excited state and to a level near to the ionization limit, from where collisional ionization took place in the air/acetylene flame to ionize the excited strontium atoms as shown in figure 3.7.

3.6.1 Selectivity

We demonstrated the selectivity of laser ionization by blocking the first exciting laser beam (460 nm) to see the intensity of the signal and we could get no signal at all, which is an indication that there were no atoms excited to populate the first excited state by the second laser beam (554.331 nm). Blocking the second exciting laser beam (554.331 nm) showed a very small signal which shows that the atoms populated to the first excited state might have been ionized by chance via collision. Moreover, if we replace the Sr solution with water, we didn't obtain any signal and this implies that we were successful in tuning the

laser beam to match the desired Sr transition. Hence this indicates the selectivity of laser ionization.

3.6.2 Influence of the Electric field strength between the electrodes

Increasing the applied high voltage also increased the electric field between the electrodes. At low voltage, the strength of the electric field is low and this results in poor collection of the charged particles created.

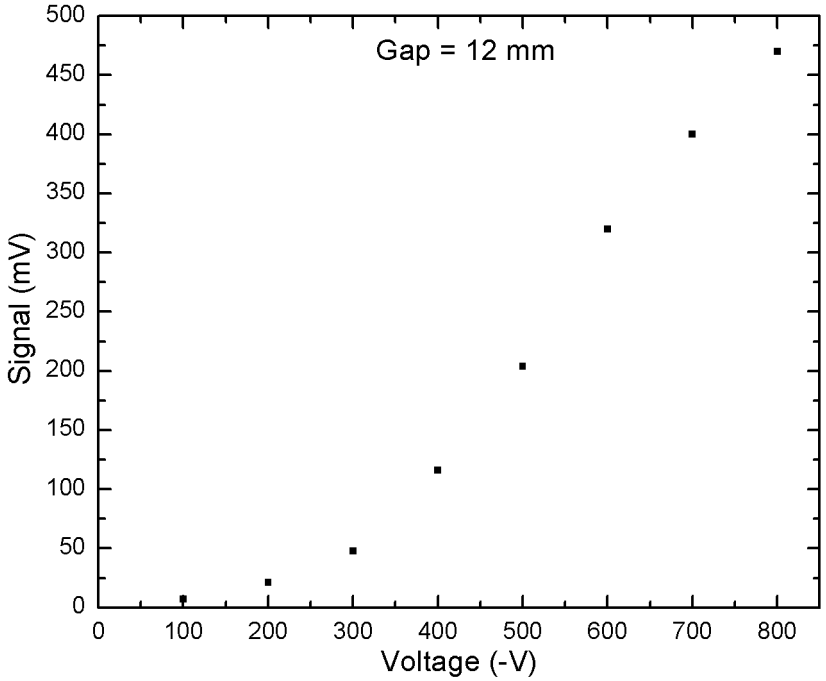

FIG. 3.8. Variation of signal amplitude with applied negative voltage.

Figure 3.8 shows the signal amplitude obtained from the solution of strontium at 1% (10000 ppm). The gap between the electrodes was kept constant at 12 mm while the applied voltage was varied from 100 V to 800 V. The graph shows that more of the charged particles created are collected as the applied voltage is increased. As this voltage is increased, the collection of charged particles should increase until it reaches a certain saturation voltage where it appears that all charged particles created are collected. However figure 3.8 shows that the Sr concentration of 1% was probably too high, so that all the charged particles

could not be collected even with the highest voltage reached of 800 V.

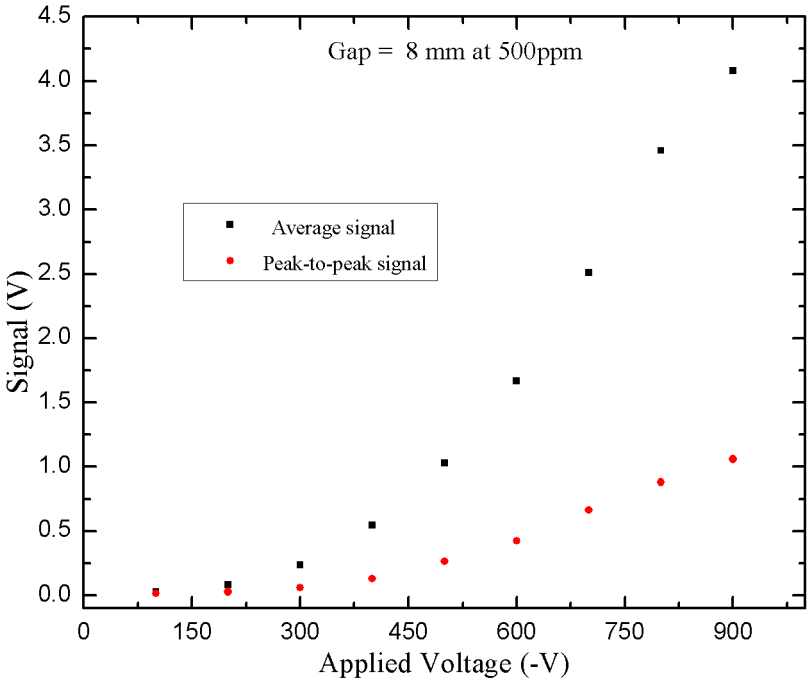

FIG. 3.9. Variation of signal amplitude with applied negative voltage at 500 ppm solution of Sr.

Figure 3.9 shows the signal obtained when the diluted Sr solution of 500 ppm was used while the gap between the electrode was kept constant at 8 mm. It shows that when the applied voltage was increased up to 800 V the collection of the charged particles created was still not adequate.

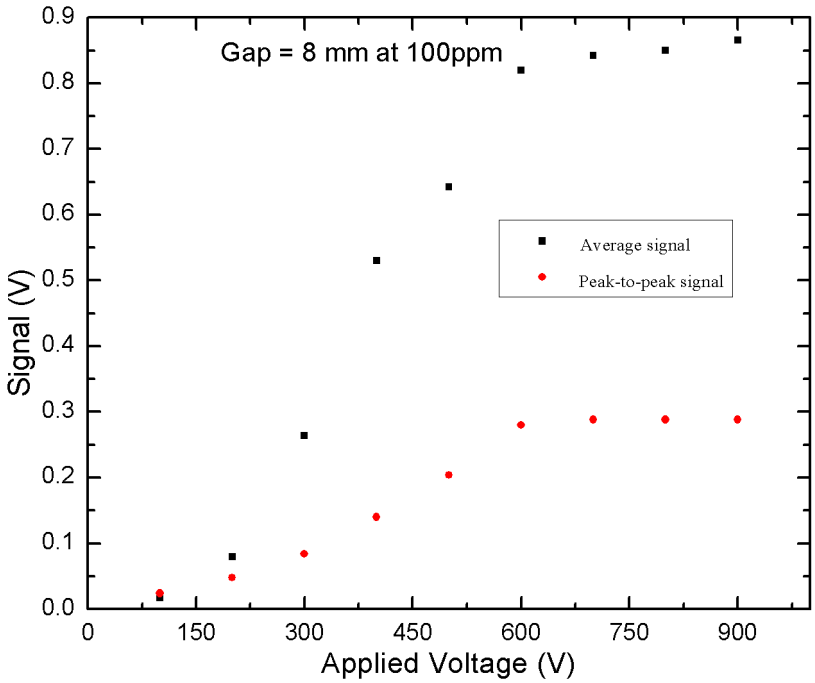

FIG. 3.10. Variation of signal amplitude with applied negative voltage at 100 ppm solution of Sr.

Figure 3.10 shows the signal obtained after further diluting the concentration of the strontium to 100 ppm, which shows that at this concentration all the charged particles created were collected i.e. from 600 V upwards the signal is saturated, which shows that all particles were collected.

3.6.3 Influence of gap between electrodes

Increasing the gap between the electrodes reduces the rate at which the charged particles and ions created are collected. As the electrode gap is increased at constant applied voltage, the strength of the electric field gets weaker, which means fewer charged particles will be collected.

Figure 3.11 shows the signal obtained by varying the electrode gap at constant applied voltage. It shows that increasing the gap between the electrodes reduces the number of charged particles collected, i.e. a smaller number of charges created reaches the electrodes due to the bigger gap.

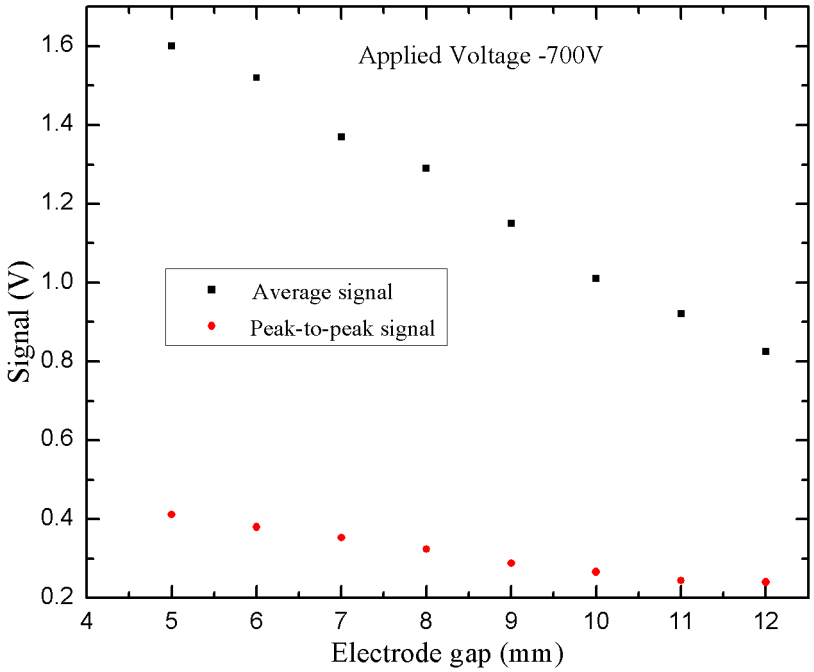

FIG. 3.11. Variation of gap between the electrode 100 ppm solution of Sr at 700 V.

3.6.4 Efficiency

Ionization efficiency is defined as the probability that an excited atom will be ionized before returning to the ground state. In reference [23] Ove Axner calculated the ionization efficiency of the first excited state of strontium (460 nm) to be 5% using the Boltzmann factor $exp(\frac{\Delta E}{\mathrm{kT}})$ where ΔE is the energy needed for ionization of the excited atom, i.e. the energy deficit: ($\Delta E = E_{ion} - E_2$, where E_{ion} is the energy of the ionization limit and E_2 the energy of the upper laser connected state [23]). They also found that the ionization efficiency for excited atoms close in energy to their ionization limit (states with energies within 1 kT, where k is the Boltzmann constant and T is temperature) is close to unity while those with an excited state of energy approximately 2.5 kT (around the excited state 6p) below the ionization limit was 50%.

In this work the following assumptions were made in calculating the amount of Sr solution going into the flame:

i. that the uptake rate was 5 ml of sample per minute;

ii. that 10% was aspirated in the flame and the rest went to the drain;

iii. therefore only 0.5 ml went to the flame per min.

If 1000 ml contains 100 μg of Sr, that means 1 ml contains 0.1 μg. Therefore in 0.5 ml there is 5.00×10^{-8} g of Sr. The 87.65 g of Sr (the molar mass) contains 6.023×10^{23} atoms (Avogadro number). Therefore 5×10^{-8} g contains 3.44×10^{14} atoms of Sr. Since the Sr atoms are spread through the flame and the flame is spread all over the burner head, this means there are some factors that must be taken into consideration like the flame speed which determines the height and the thickness of the flame. Another important factor is the diameter of the laser beam which will tell us the number of atoms "hit" by the laser beam.

Using the peak-to-peak signal obtained with the 100 ppm solution of strontium at 8 mm electrode gap we found the following: the peak-to-peak signal was 0.288 V and the resistor used was 50 kΩ. The current obtained is given by ohm's law.

Using this equation we found the current that passes through resistor is 5.76 μA. The laser pulse length is 20 ns. The charge equation is given by

$$Q = It \tag{3.3}$$

Using this equation we found the collected charge is 1.15×10^{-13} C. The number of electrons collected (N) is given by the following equation

$$N = \frac{Q}{e} \tag{3.4}$$

Where e is electric charge given by -1.6×10^{-19} C and Q is charge calculated above, therefore the number of electrons collected is 7.20×10^{5} electrons/pulse.

The volume of the flame is given by

$$V_f = 1600 \quad \text{mm} \times 100 \quad \text{mm} \times 10 \quad \text{mm}$$

$$= 1.6 \times 10^6 \quad \text{mm}^3$$

This means 1.6×10^6 mm^3 contains 3.44×10^{14} atoms. We can get the number of atoms in the laser beam using the following. Since we know that the number of atoms aspirated in the flame and with a laser pulse length of 20 ns, the number of atoms that could be radiated by the laser light is

$$20 \times 10^{-9} \times 3.44 \times 10^{14} = 6.88 \times 10^6 \text{ atoms}$$

This gives the number of atoms in the laser beam. The efficiency is given by the following equation:

$$\text{Efficiency} = \frac{\text{Number of electron collected}}{\text{Number of atoms present in the flame}} \times 100 \tag{3.5}$$

$\therefore$ the efficiency was found to be 0.1046 or 10.46%.

Chapter 4

Time-of-Flight Mass Spectroscopy

4.1 Introduction

In this experiment, selective ionization of indium atoms in a vacuum was attempted, with the goal to use time-of-flight mass spectroscopy to confirm that indium atoms were indeed ionized. The design and construction of an atomic beam apparatus connected to a linear time-of-flight mass spectrometer for mass separation indium will be covered as well as the principle of our spectrometer. We will conclude by discussing the results obtained using this method.

4.2 Principle of the time-of-flight mass spectroscopy

A time-of-flight mass spectrometer (TOFMS) is a crucial tool for mass analysis and it has been used with great success for a number of applications. Most TOFMSs consist of an ion source and the detector situated at the opposite ends of an evacuated tube [32]. Ions are formed in the ionization region of the source, usually by laser ionization. The charged particles created are accelerated out of the ionization region toward the detector by means of an applied electric field and separated according to their mass-to-charge ratio (m/q) in the field-free region so that ions reach the detector according to their masses (i.e. lighter first, then the heavier ones).

4.2.1 Advantages and Disadvantages

The unique advantage of TOFMS is the speed at which it can obtain the mass spectrum, i.e. in the range of microseconds (μs). This allows one to study how the relative intensities of different ions vary when source conditions are changed rapidly [33]. Another characteristic of the TOF spectrometer is that it can record the entire mass spectrum for the accelerating pulse.

The main disadvantage of the TOFMS is the limited resolution. Even though these instruments are not designed to give the precise mass measurements possible with more complex, slower, lower-intensity magnetic TOF spectrometers, they must separate adjacent mass units sufficiently well to permit accurate relative intensity measurements [34]. The TOFMS have the following properties:

4.2.2 Flight time

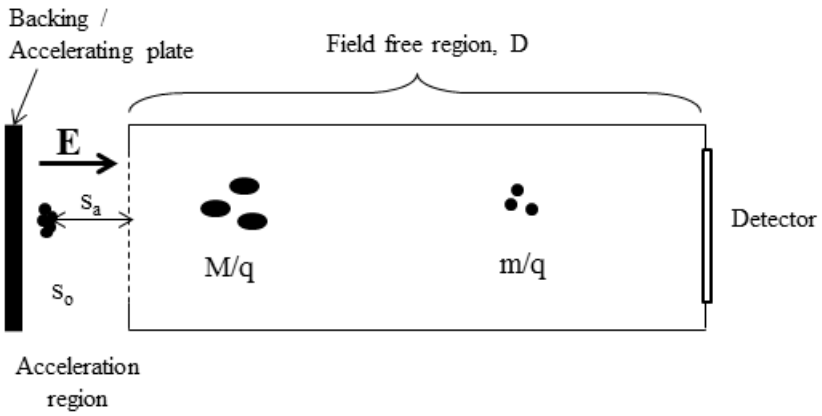

FIG. 4.1. Single linear time-of-flight spectrometer.

In figure 4.1, a voltage is applied to the backing plate to accelerate the ions created in an ionization region defined by a grounded grid. The created ions are accelerated by this electric field until they enter the field-free region(D) where they are separated according to their mass-to-charge ratio, with the lighter ions reaching the detector before the heavier ones. Since ions are formed in the gas phase, they are subjected to a Boltzmann distribution of initial velocity (u_o). The ions created are moving in all directions and are guided by an electric field; those ions which are moving toward the detector arrive before ions which

were initially moving away from the detector. The latter ions are first decelerated to zero velocity before they are re-accelerated and pass through their initial position. The time for this to occur is called turn-around time $t_{\pm}$ (the signs specify the direction of the ion with respect to the detector) [33].

To get the time an ion takes from the point of creation until it reaches the detector, the following has to be considered. The ions moving in the same direction and having a distribution of masses with approximately the same kinetic energy will have the corresponding distribution of velocities in which the velocity is inversely proportional to the square root of m/q. If we consider the situation of ions formed at the same time under the influence of an electric field, they begin their acceleration from rest at the same time. Knowing that the acceleration a is given by the following expression

$$a = \frac{du}{dt} \tag{4.1}$$

then to find the velocity (u) of these ions we integrate equation (4.1) with respect to u, which gives

$$u = \int \frac{Eq}{m} dt \tag{4.2}$$

($F = Eq$, $F = ma$ then $a = \frac{Eq}{m}$ where E is the electric field strength, F is the force, q is the charge and m is mass). From equation (4.2) gives the velocity as

$$u = u_o + (\frac{Eq}{m})t \tag{4.3}$$

From equation (4.3) the time is found to be:

$$t = \frac{u - u_o}{E}(\frac{m}{q}) \tag{4.4}$$

If we assume that all ions are formed at same time and at the same distance from the detector, and setting $u = -u_o$ (from equation (4.4)), then we can obtain the turn-around

time where the sign specifies the direction:

$$t_{\pm} = \frac{2|u_o|}{Eq} \tag{4.5}$$

Knowing the initial translational energy $U_o = \frac{1}{2}mu_o^2$, then the turn-around time can be expressed as a function of this initial transition energy as follows:

$$t_{\pm} = \frac{2\sqrt{2mU_o}}{Eq} \tag{4.6}$$

This implies that two ions with same initial speed but moving in opposite direction will reach the same final velocity after acceleration but they remain separated by the turn-around time until the detector is reached. If the drift region is increased, this separation in time becomes smaller relative to the total flight time. Equation (4.6) also shows that the turn-around time can be decreased by increasing the strength of the accelerating field.

The time for an ion to travel a distance s from initial position s_o can be obtained from the following integration and quadratic equation (obtained from equation (4.3))

$$s = \int u dt$$

$$s = s_o + u_o t + \left(\frac{1}{2}\right)\left(\frac{Eq}{m}\right)t^2 \tag{4.7}$$

Solving equation (4.7) for t and substituting $u_o = \sqrt{\frac{2U_o}{m}}$, we obtain

$$t = -\frac{\sqrt{2mU_o}}{Eq} \pm \frac{\sqrt{2m(U_o + Eqs)}}{Eq} \tag{4.8}$$

The physical meaning of this equation is that it shows the space time trajectory of an ion passing through $t = t_o$ with an initial velocity (u_o). If the initial velocity of the ion is $-u_o$ this will give the equation for time t_a to reach the drift velocity (is an avarege velocity that a particle such as an ion attains due to an electric field)

$$t_a = \frac{\sqrt{2m(U_o + qEs)}}{Eq} \pm \frac{\sqrt{2mU_o}}{Eq} \tag{4.9}$$

In equation (4.9) the turn-around time is apparent in the second term. Setting the distance from s_o to the beginning of the drift region as s_a, the drift energy is $(U_o + qEs_a)$ from which the drift velocity is

$$u_D = \sqrt{\frac{2(U_o + qEs_a)}{m}} \tag{4.10}$$

Thus for a drift-length D, the drift time is

$$t_D = \frac{D}{2}\sqrt{\frac{2m}{(U_o + qEs_a)}} \tag{4.11}$$

The total time it take an ion to reach the detector can be expressed by combining equations (4.9) and (4.11) and this gives a well-known equation calculated by Wiley and McLaren in 1955 [33, 34].

$$t = \frac{\sqrt{2m}[\sqrt{U_o + qEs_a} \pm \sqrt{U_o}]}{qE} + \frac{\sqrt{2m}D}{2\sqrt{U_o + qEs_a}} \tag{4.12}$$

The effect of the turn-around time can be decreased by increasing D, but long drift-length also introduce technical problems such as the need to increase detector size and the pumping speed of the vacuum system.

4.2.3 Spatial Resolution

Spatial focusing (the ability of the detector to differentiate between two objects in space which are separated by a small distance) depends on the fact that ions with a shorter distance to travel to the detector will acquire less energy and they will be overtaken by ions that lie far away from the detector [34]. Because these ions spend more time in the accelerator region, they reach drift velocity faster and have a shorter drift time. In equation

(4.12), if $U_o = 0$ then we can obtain dt/ds_a [33]:

$$\frac{dt}{ds_a} = \sqrt{\frac{m}{2qEs_a}}\left(1 - \frac{D}{2s_a}\right) \tag{4.13}$$

This function eq. (4.13) shows that t reaches the minimum when $D = 2s_a$ and the spatial focusing is thus achieved at a plane located at a distance of $2s_a$ along the drift region. This focusing condition is the same for all ions and is independent of the total energy of the system.

4.2.4 Energy resolution

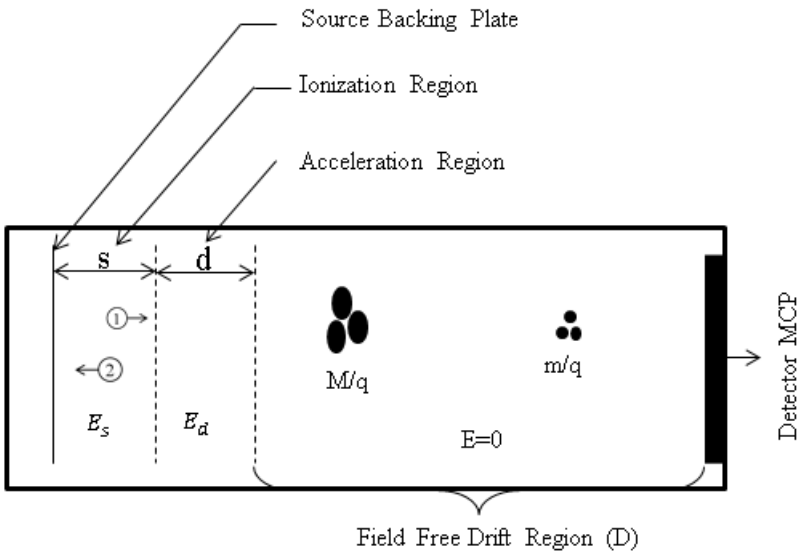

FIG. 4.2. Two-stage linear time-of-flight mass spectrometer. E_d and E_s are the electric fields applied in regions d and s respectively.

The double field system shown in 4.2 [33] brings ions to their maximum energy quite fast compared to a single field. The distribution effect of initial energy U_o is reduced because it is a smaller percentage of the energy which determines the velocity at each point [33]. So to examine the effect of the initial velocity, it is convenient to consider two ions formed at the same initial position but moving in different direction as in figure 4.2. Ions that move away from the detector decelerate due to E_s until stopped and accelerate again in the direction of a detector and their motion is identical to those ions that started in the

direction of detector, but they only lag behind by the turn-around time.

4.2.5 Mass Resolving Power

The resolution of the time-of-flight mass spectrometer is needed to distinguish two ions of different masses and the maximum resolvable masses depends on the initial space- and energy-distribution functions. In most time-of-flight experiments, ions are brought to keV translational energies over a distance of a few millimetres and the time that ions drift in a field-free region of about a metre is much larger than the time of acceleration. In a spectrometer it is conventional to measure resolving power by the ratio of $\frac{m}{\Delta m}$ where Δm is a mass difference. In TOFMS it is convenient to work in the time domain, thus the resolving power can be measured in terms of $\frac{t}{\Delta t}$ as follows:

since $m \propto t^2$, i.e. $m = At^2$ where A is just a proportionality constant, therefore

$$\frac{dm}{dt} = 2At = \frac{2m}{t}$$

$$\therefore \frac{dm}{m} = \frac{2dt}{t}$$

therefore the mass resolving power of the TOFMS can be given in the time domain as

$$R = \frac{m}{\Delta m} = \frac{t}{2\Delta t} \tag{4.14}$$

where $2\Delta t$ is full width at half maximum (FWHM) of the peak, and Δm has replaced the masses of the two separate ions. This shows that the resolution for the given mass is based on time-of-flight and peak width and it is clear that the resolution can be maximized by increasing the time-of-flight (either by a long drift length or low acceleration potential) or by narrow peak width.

4.2.6 Result obtained from previous studies using TOF

As an example, the following figure (4.3) shows the results obtained using the time-of-flight mass spectroscopy where the laser pulse is used as reference to measure the abundance of two lithium isotopes. Muhammad Saleem has shown that the lighter ions of lithium (Li^6) arrive faster than the heavy lithium (Li^7) ions [32].

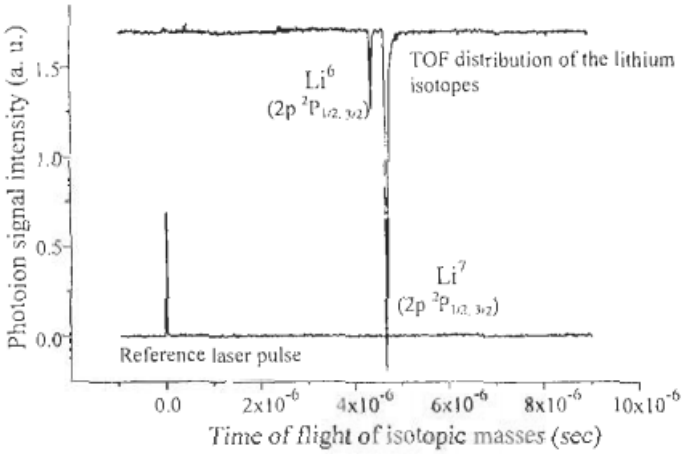

FIG. 4.3. TOF distribution of lithium isotopes, Li^6 and Li^7, produced as the result of photo-ionization.

Figure 4.4 shows the behaviour of the TOF detector for measuring the relative abundance of lithium isotopes as function of applied voltage, which shows that increasing the voltage applied on the detector also increase the signal intensity of the two lithium isotopes [32].

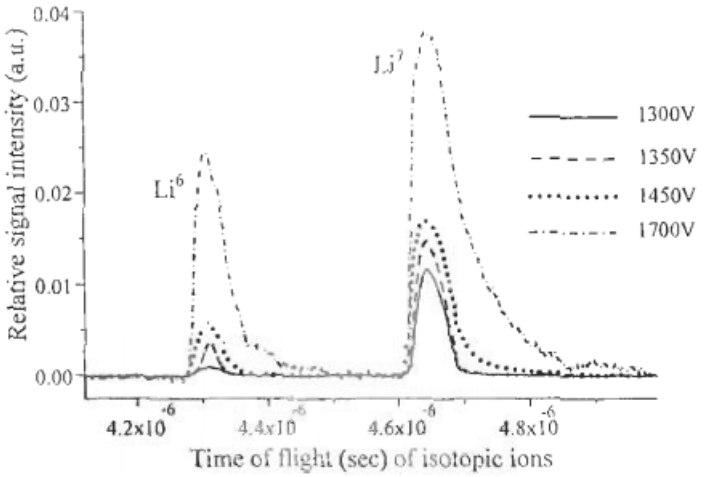

FIG. 4.4. Relative signal intensity of the lithium isotopes at different TOF detector applied voltage.

4.2.7 Choice of atomic beam

Indium was chosen because it is an element that would be produced in the fission of uranium, it is a metal (with 49 electrons) with a very low melting point of 156.61°C (compared to its group metals gallium and thallium) which make it easy to produce an atomic beam without using high temperature. Natural indium has one stable isotope (^{113}In, mass = 112.904 amu) and one radioactive isotope (^{115} In, mass = 114.903 amu with a half-life of 4.41×10^{14} years which beta decays to ^{115}Sn) with a long half-life which comprises 95.7% of natural occurring indium while the stable isotope comprises 4.3 %. Indium has two ground state configurations, which are $1s^2 2s^2 2p^6 3s^2 3p^6 3d^{10} 4s^2 4p^6 4d^{10} 5s^2 5p^2 P^0_{1/2}$ and $1s^2 2s^2 2p^6 3s^2 3p^6 3d^{10} 4s^2 4p^6 4d^{10} 5s^2\ ^1S_0$, with ionization energies of 46670.11 cm^{-1} and 152199 cm^{-1} respectively. Its boiling point is 2000°C which is higher than that of thallium but lower than that of gallium showing the opposing trend to that showed by the melting points.

4.3 Design of the ToF apparatus

An existing time-of-flight chamber was used for our experiment. This time-of-flight chamber had been used for either gas or molecular analysis. The chamber had a small aperture

to inject a sample to be analysed in the ionization region where the sample was irradiated by laser light and the ions created were accelerated twice before they enter the free-field region. This TOF originally had a single turbo-pump as shown in figure 4.5.

However, to make the TOF chamber suitable for the ionization of heavy elements such as Indium, or those produced by fission, it had to be modified extensively. We designed an atomic beam source (oven system) with a good set of collimators to produce a collimated atomic beam. This required the additional of a second turbo-pump.

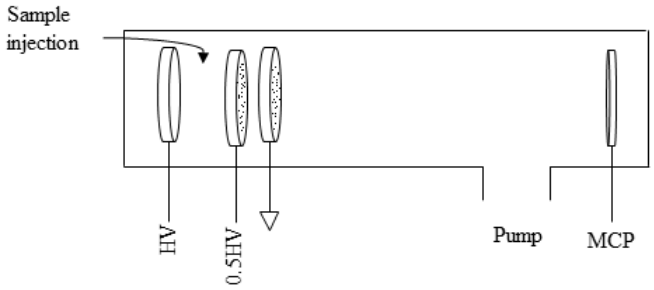

FIG. 4.5. The old TOF used for gas and molecular analysis.

A well-collimated atomic beam is a powerful tool for investigation of fundamental properties of atomic nuclei. The newly designed atomic beam system consisted of an oven containing a source of atoms, an exit hole and a set of apertures to attain a well-collimated beam. High directivity atomic beams are used for different purposes such as isotope separation by the laser method, laser selective excitation or ionization of ions in a TOF mass spectrometer. One advantage of producing a well-collimated atomic beam is to reduce the random motion of atoms which may result in Doppler broadening, which will cause the broadening of spectral lines; another is to prevent unwanted deposits around the chamber.

4.3.1 Fabrication

Our TOFMS consists of a vacuum chamber (oven), a grid assembly, a flight tube and the ion detector at the end of the tube. The grid assembly is composed of a backing (accelerating) plate which is a flat circular stainless steel plate and two grids G_1 and G_2. High voltage is applied to the backing plate and half the voltage is applied to the first grid (G_1), while the second grid (G_2) is grounded (see figure 4.7).

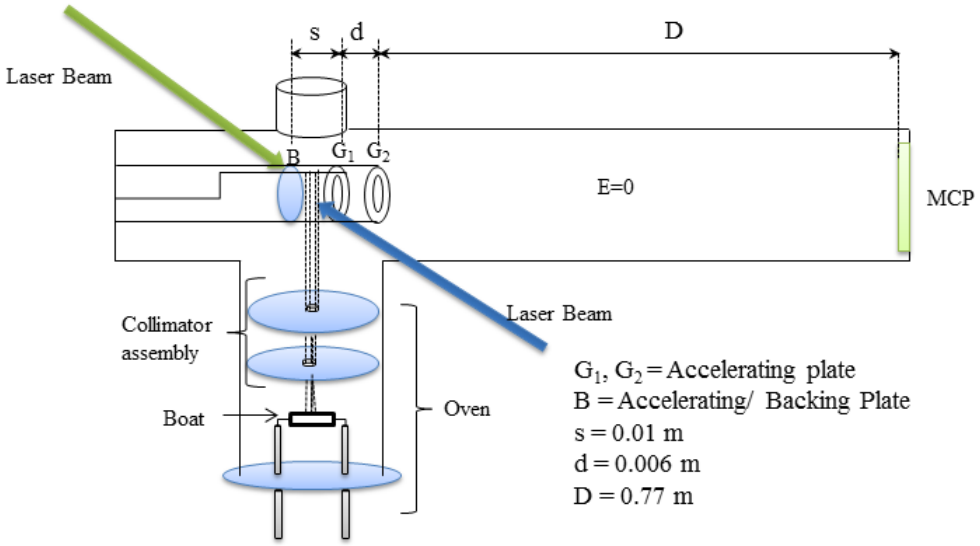

FIG. 4.6. Schematic diagram of the TOFMS.

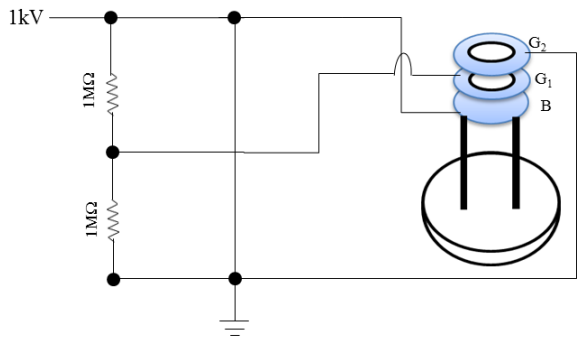

FIG. 4.7. Ion acceleration grid assembly with voltage divider.

The entire grid assembly is mounted on a flange and installed in a flight tube. Vacuum of the order of $\approx 10^{-6}$ torr was maintained on our system by two turbo-pumps. The atomic beam source was placed right beneath the ionization region of the flight tube. The ions are produced as a result of laser-atom interaction, then accelerated twice to enter the field-free region where they are separated according to their mass-to-charge ratio(m/q) and detected by a Micro Channel Plate (MCP) detector, (described later), at the end of the flight tube.

4.3.2 Atomic Source

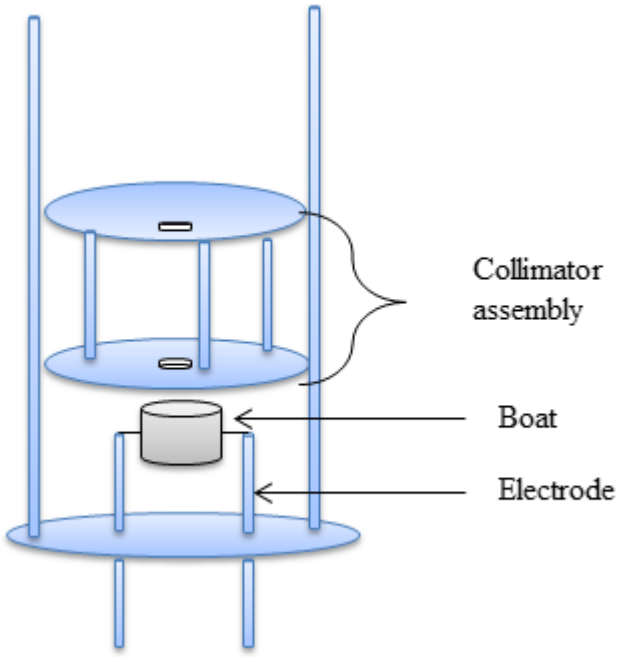

(a) Complete schematic diagram of the atomic beam source.

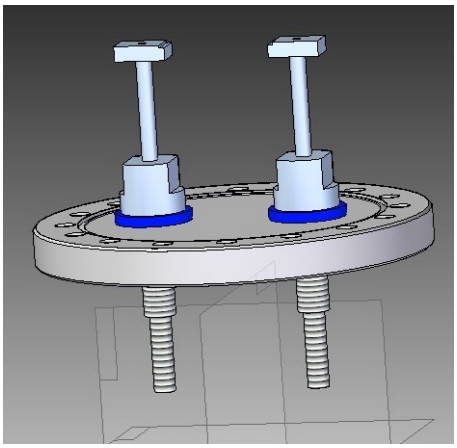

(b) Electrodes used tosupply power to a boat.

(c) Electrode with water cooled system.

(d) Collimator disks.

FIG. 4.8. Details of the oven system.

The atomic source is a cylindrical stainless steel oven and the design of some of the oven parts is shown schematically in figure 4.8(a). The material to be evaporated is placed in a boron chloride or quartz "boat" which can be heated electrically. The design of the boat (4.9) was chosen because it can be electrically heated slowly which can make our

sample last for a longer period. Two electrodes are mounted on the bottom flange of the oven to provide high current to heat the boat 4.8(b), while the boat is clamped on top of the two electrodes which are kept cool using an external water cooling circuit 4.8(c). The collimator consists of two stainless steel disks with a hole at the centre of a diameter 3.5 mm 4.8(d). The two disks can be adjusted to get the correct distance between the boat exit hole and the collimator hole. Stainless steel was chosen for other components because it is a good vacuum material and this design of the oven was used because it allows replenishment of the sample without disturbing the entire arrangement and alignment of the whole experimental setup.

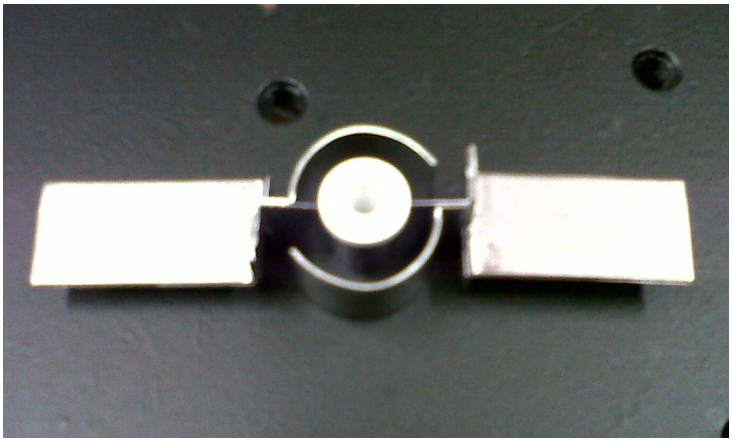

FIG. 4.9. Boron chloride boat.

4.3.3 Ion Detector

The temporal response of the detector to the ion arrival can be an important contributor to the peak width of the obtained signal. Re-arranging equation 4.14 , we get

$$\frac{\Delta m}{m} = \frac{2\Delta t}{t}$$

Therefore, to obtain a mass resolution of better than 1%, we need to have a time resolution of better than 0.5%. Next, we consider the expected time-of-flight in our system.

4.3.3.1 Time-of-flight

To estimate the time it takes for an ion to reach the detector from the point of creation, one needs to know the following aspects about the experimental setup.

• Total length TOF tube = 0.940 m

• Since we have a double linear TOF system, we have two acceleration regions and an electric-field-free region knowns as a drift region:

(a) ionization region = 1 cm = 0.01 m

(b) second region 0.6 cm = 0.006 m

(c) drift length = 0.77 m

The time of flight of the ions created can be estimated using the Willey McLaren equation 4.12 as described in section 4.4. From the properties of our time-of-flight system, the electric field between the acceleration region as shown in figure 4.6 is given by this equation

$$E = \frac{V}{d} \tag{4.15}$$

where V is the voltage (in volts) applied and d (in metres) is the distance between the grids as shown in figure 4.7 and 4.15 gives

$$E_s = 1 \times 10^5 \text{ V/m}$$

$$E_d = 8.33 \times 10^4 \text{ V/m}$$

As stated in section 4.2.7, the two stable isotope of indium with the following masses will have the following time-of-flight according to 4.12.

$$m_{112amu} = 1.88 \times 10^{-25} \text{ kg}$$

$$m_{114amu} = 1.92 \times 10^{-25} \text{ kg}$$

$$\Rightarrow t_{112amu} = 16.19\mu s$$

$$\Rightarrow t_{114amu} = 16.34\mu s$$

Thus, the ion-detector will need to have a time resolution of better than $0.005 \times 16\mu s \simeq 80$ ns to resolve the two isotopes of indium.

4.3.3.2 Micro-channel Plate Detector

In our experiments we used a micro-channel plate because of its fast time response and high sensitivity.

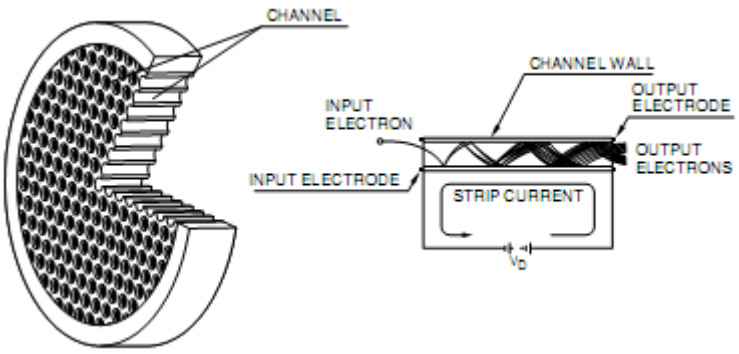

FIG. 4.10. Schematic structure of an MCP and the principle of multiplication [35].

An MCP is an array of a great number of channels arranged parallel to each other and formed in a thin disk of glass. Each channel has an internal diameter ranging from 6 to 20 microns with an inner wall processed to have the proper electric resistance and secondary emissive properties. This property allows each channel to be considered as a continuous dynode structure that acts as its own dynode resistor chain [36]. The cross section view of channels and the principle of multiplication is illustrated in figure 4.10, which shows that when a primary electron strikes the wall of a channel it produces secondary electrons. The voltage V_D applied across the end of the MCP produces an electric field which accelerates the secondary electrons which then multiply by producing further secondary electrons [35]. This process repeats over a thousand times along the channel, and as a result, a large number of electrons are emitted at the output end.

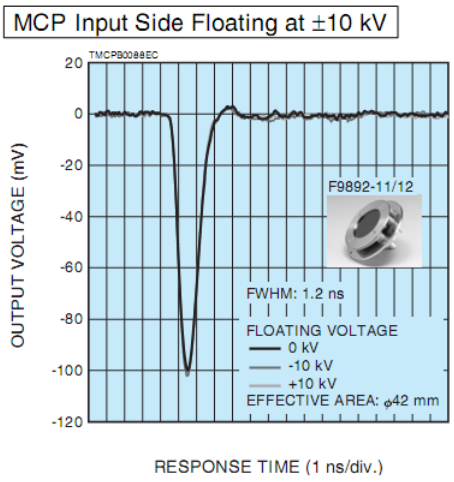

FIG. 4.11. MCP signal [37].

MCPs are quite different in structure from other photomultipliers and this gives MCPs outstanding features such as high gain, compact size, fast response time as shown in figure 4.11, two-dimensional detection with high spatial resolution, sensitivity to charged particles and low power consumption.

Our MCP assembly was in a chevron configuration, with two plates back-to-back, to provide gains of up to 10^7. The circuit for the MCP is shown below; a voltage divider provided about 2kV across the MCP. Electrons emerging from the back of the plates were collected at the anode to form the signal. To ensure a field-free drift tube, a grounded grid was placed in front of the assembly.

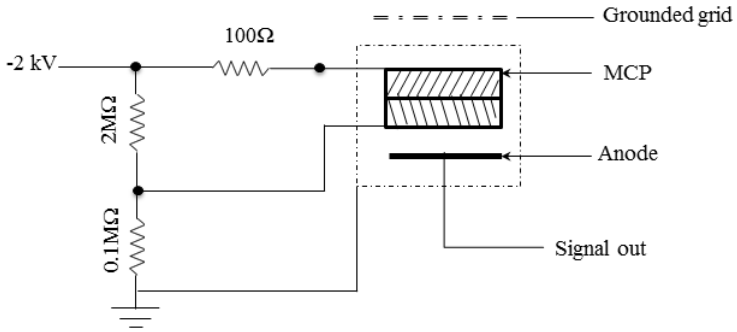

FIG. 4.12. Electronic circuit for the voltage divider used on the MCP.

4.4 Experimental setup

4.4.1 Ionization Schemes

In the past, resonant laser spectroscopy has been applied in the analysis of In atoms using different schemes where atoms are being excited from the one of the two ground state configurations. The schemes used to study In atoms are similar to the ones mentioned in section 2.1.1. Due to the availability of an excimer laser, dye-laser and required dyes, we chose two laser beams to excite and ionize indium atoms using the transitions given in figure 4.13

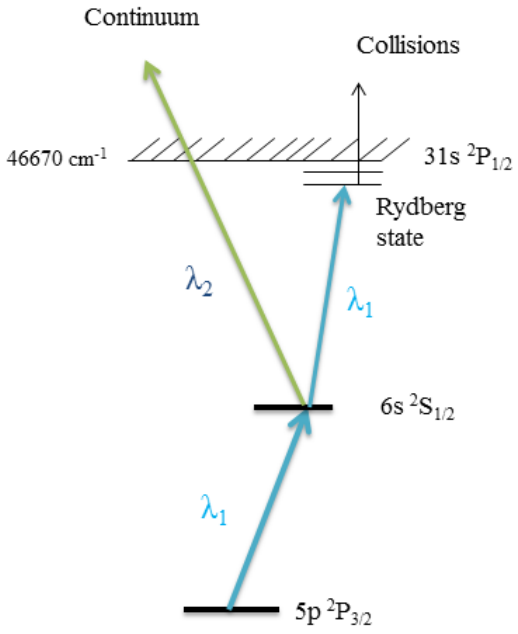

FIG. 4.13. Excitation wavelengths used for indium excitation and ionization, where $\lambda_1 = 451$ nm and $\lambda_2 = 308$ nm [38].

4.4.2 Experimental procedure

The following figure 4.14 shows the schematic diagram of the experimental setup including the lasers. It includes the vacuum chamber built with an atomic beam source and time-of-flight mass spectrometer, a dye-laser, an excimer laser and a digital storage oscilloscope for spectrum analysis. The excimer laser (lasing at 308 nm(25 mJ)) was used to pump the dye-lasers (which produce 451 nm(0.78 mJ) for excitation) and to ionize the atoms.

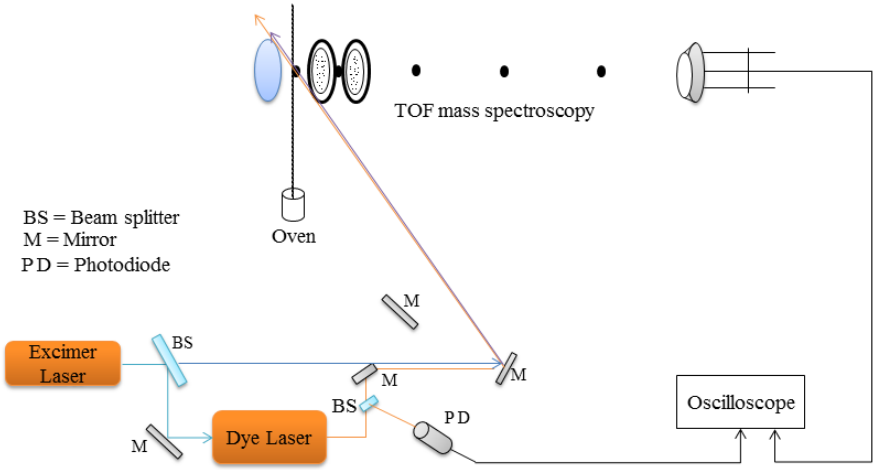

FIG. 4.14. Time-of-flight mass spectrometer setup.

FIG. 4.15. Photograph of the setup.

To generate the atomic beam, a sample of indium was heated in an oven by applying high current ($\approx$ 90 A) to the boat using a Hewlett-Package 6260B DC power supply, and the boat was placed precisely below the ionization region of the TOF mass spectrometer, where atoms created travel from the bottom to the top of the vacuum chamber after passing through a set of collimators.

The dye used was Coumarin 47 (to generate 451 nm) dissolved in pure solvent (method). The two laser beams were introduced into the vacuum chamber from opposite directions using the set of mirrors as shown in figure 4.6. The amount of the sample heated was restricted by the size of the boat. The indium sample was placed in the oven in a boron chloride boat and the atomic beam source was collimated to be just below the ionization region and the TOFMS used for the detection of indium ionic masses. The ions created were accelerated twice in the direction of the detector by means of applying high voltage. The time-of-flight of the ions created was measured. During the course of the experiment, the pressure was maintained at 10^{-6} torr in our system.

4.4.2.1 Ionization Probability

The setup needed to provide a reasonable signal to confirm the ionization of indium atoms. Therefore, we consider whether the ionization probability would be high enough to give a signal of sufficient amplitude.

If both conditions mentioned in section 2.2.1 are fulfilled by our laser beam, then all the atoms in the laser-atom interaction region hit by the laser beam will be ionized. To get the number of photons in a pulse, we have to know the energy of each photon, which is given by the following equation

$$E_\lambda = \frac{hc}{\lambda} \tag{4.16}$$

were h is Planck's constant, c is the speed of light and λ is the wavelength and in our case λ = 451 nm and 308 nm; then equation 4.16 gives

$$E_{(\lambda=451)} = 4.41 \times 10^{-19} \text{ J}$$

$$= 2.76 \text{ eV}$$

and

$$E_{(\lambda=308)} = 6.50 \times 10^{-19} \text{ J}$$
$$= 4.06 \text{ eV}$$

To get the number of photons (η) in a pulse we use equation 4.17

$$\eta = \frac{E_{out}}{E_{\lambda}} \tag{4.17}$$

where E_{out} is the measured output energy of the dye-laser (lasing at 451 nm) and excimer laser (lasing at 308 nm). The laser beam from the excimer was split into two beams, one used to pump the dye-laser while the other beam was used to ionize indium atoms. A 70% beam splitter was used to split the excimer laser beam and using the energy meter, 25 mJ was measured to ionize (the indium atoms) after the beam splitter and 0.78 mJ was measured from the dye-laser. This implies that each laser beam has the following of number of photons per pulse:

$$\eta_{(451)} = 1.77 \times 10^{15} \text{ photons/pulse}$$

$$\eta_{(308)} = 3.85 \times 10^{16} \text{ photons/pulse}$$

Both the 308 nm and 451 nm laser beams were carefully focussed and aligned into counter-propagating beams each of approximately 1 mm^2 area. The photon flux is then approximately 2×10^{17} and 4×10^{18} photons/cm^2/pulse for the 451 and 308 nm beams, respectively, for a pulse rate of 10 Hz. The latter of the two conditions, 2.7 and 2.8, is the most stringent, so we consider it here. To make a conservative estimate, we assume a (non-resonant) ionization cross-section of 10^{-17} cm^2. Condition 2.8 is then satisfied even for the low-intensity 451 nm laser beam:

$$\sigma_I \phi = 10^{-17}\text{cm}^2 \times 2 \times 10^{17}/\text{cm}^2$$
$$= 2 > 1$$

To calculate the number of atoms ionized per second, we need the intensity of the atomic beam from the ion source. First, some details:

• The size of the boat:

diameter = 4 mm

height = 13 mm

• The amount of the sample heated

Indium = 0.6508 g, and 115 g of indium contains 6.022×10^{23} atoms, which means that 0.6508 g contains 3.39×10^{21} atoms. If we evaporate for 5400 seconds, (90 minutes) then the number of atoms evaporated per second is 6.28×10^{17} atoms per second.

• Collimator assembly.

The diameter of the collimator disks is 4 mm. Assuming atoms are scattered uniformly in all upward directions when they come out of the boat, the second collimator defines a solid angle that accepts 4×10^{-4} of the total flux. Hence, the atomic beam contains 2.4×10^{14} atoms/s, but by the time it reaches the laser interaction region, it would be much larger in area, (about 13 mm in diameter). The average velocity of the atoms, according to the Boltzman equation, and assuming a temperature just above the boiling point (2300°K) is of the order of 1000 ms^{-1} (or 1 $mm/\mu s$). During a laser pulse, (of 1 mm^2 area and 10 ns duration) approximately 10^7 atoms will enter the exposure area. Since condition 2.8 is fulfilled we expected most of these atoms to be ionized. This would correspond to a large pulse in the MCP, which is sensitive to single atoms.

Finally we note that the laser pulse length was of the order of 10 ns. Since the speed of light is approximately 30 cm/ns, small differences in path-lengths between 451 and 308 nm beams can be neglected.

4.4.3 Data Acquisition

Figure 4.16 represents the circuit diagram of the experimental setup. The signal from the MCP was fed to oscilloscope. A photo diode was used to trigger the oscilloscope and to

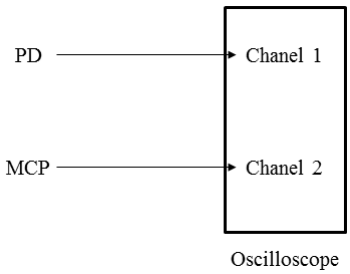

FIG. 4.16. Circuit digram of the experimental setup.

measure the laser pulse as a reference pulse.

4.5 Results and Discussion

4.5.1 Experimental result

Two processes were used to excite indium atoms from the ground state to an excited state. These processes are similar to the one mentioned in section 2.1.1 figure 2.2. Indium can be excited using two steps in a single-frequency field where $\lambda_1 = \lambda_2$, and in a double-frequency field $\lambda_1 \neq \lambda_2$. Figure 4.13 shows the schemes used for indium ionization [38].

4.5.1.1 Flight time

The time-of-flight signal of indium ions is shown in figure 4.17 where the laser pulse signal is used as reference pulse to measure the time-of-flight of indium ions. The time-of-flight of indium ions can be measured accurately with a TOF mass spectrometer but in this case we had a problem with our MCP detector, which resulted in poor measurements. To get accurate mass separation of the indium isotopes, the rise time of the detector signal should be smaller than 80 ns.

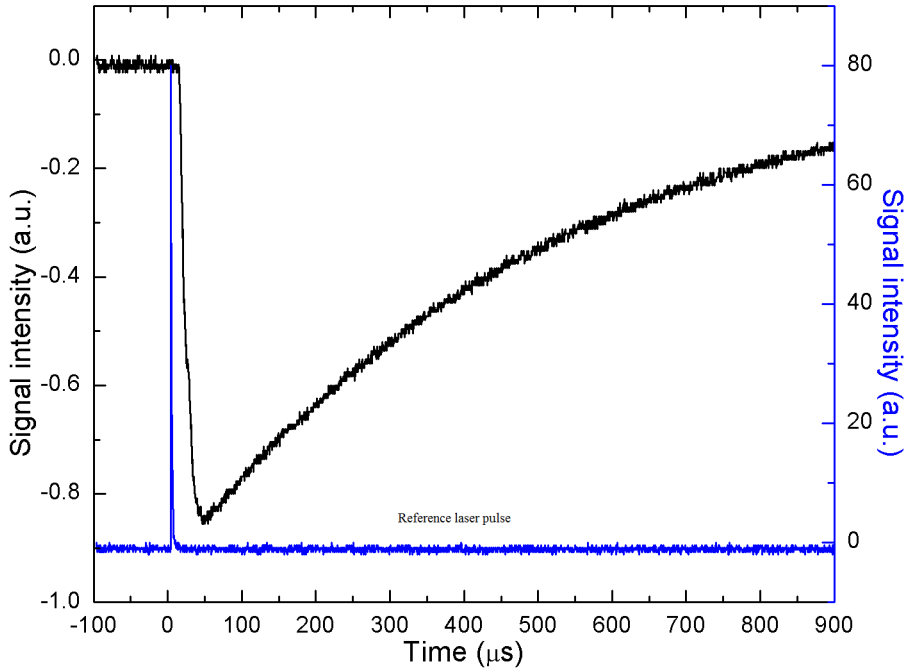

FIG. 4.17. Time-of-flight of indium atom.

The signal has a slow rise time and long tail, which was unexpected. To demonstrate ionization of our sample (indium), the following observations were noted. When the oven was switched off, no signal was observed using either 451 nm or 308 nm beams by themselves and even if both wavelengths (451 and 308 nm) were used. Turning on the oven and using the 451 nm beam, no signal was observed on the oscilloscope. If we used the excimer laser alone, a signal was observed which means we were able to ionize something from the oven, but the ionization using the excimer laser is not selective. Using both wavelengths, we observed a signal as shown in figure 4.17. Since our detector was not functioning properly, this resulted in poor time resolution of our spectrum. Taking the average of the rising slope gives the flight time of the ion signal which is the time at which indium ions hits the detector. This gives t = 26.63 μs $\pm$ 16.45 μs. The difference between expected (time calculated in section 4.3.3.1) and measured times is 10.29 μs.

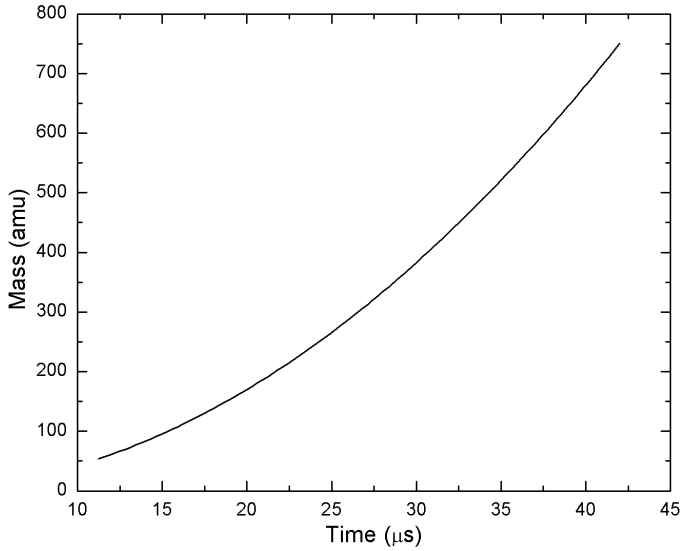

FIG. 4.18. Mass against time-of-flight of the measured ions.

In figure 4.17, the signals start at 11.15 μs and ends at 42.11 μs. To find what mass interval this corresponds to, the McLaren equation (4.12) was used, which in this case is approximately:

$$m = 0.43t^2 \tag{4.18}$$

where t and m represents time and mass, respectively.

Plotting the calculated mass against the time-of-flight of the signal, we obtained figure 4.18. This figure indicates the shortest time-of-flight corresponds to a heavy element with a mass above 53 amu. This is entirely compatible with the ionization of Indium, and is unlikely to be anything else, as most contaminating residual gases have lighter mass.

Because of the poor time-resolution, the MCPs were removed from the system and checked. They were found to be cracked. Another set of (used) MCPs were acquired and placed in the chamber. The previous observation that ionization was observed with the excimer beam alone, suggested that its intensity may previously have been too strong. In the new setup, collimators were used to reduce the beam dimension and intensity. The test was repeated; unfortunately, in this instance no signals were observed from the MCP. A large current being drawn from the replacement MCPs implied a short circuit across the plates.

Opening revealed another cracked MCP. The time and expense required to import new, replacement MCPs precluded further work on the project.

The poor time resolution of the spectrum has prevented us from proving conclusively that our goal (selecting ions according to their atomic number) has been achieved. However, with a functioning detector, laser ionization of nearly any element using on similar systems has been achieved successfully.

Chapter 5

Conclusion

5.1 Summary

The main aim of this project was to develop and demonstrate a method that will be able to selectively ionize any element of interest. This technique must work perfectly for stable isotopes as well as short-lived rare isotopes, and it must work well with different techniques for the production of radioactive-ion beams.

The theory behind the production of radioactive-ion beams using modern (ISOL) technologies was comprehensively discussed including the techniques employed for selective ionization. Ionization mechanisms that are employed in the ISOL system for the production of RIBs were fully discussed including the application of resonant laser ionization. For high efficiency and selectivity in the production of RIBs, different method were given and discussed. Laser-atom interactions were treated including different methods applied for high selectively and efficiency such as multi-step or multi-photon ionization, and it was shown that multi-step ionization yields higher efficiency and selectivity compared to single-step ionization which suffers from poor transition probability.

The design and construction of the time-of-flight mass spectrometer for laser ionization and detection of atoms were shown in detail and also the oven system for the production of the atomic beam. Laser ionization was demonstrated using two different methods, i.e. laser-enhanced ionization and time-of-flight mass spectroscopy. In both of these method multi-step ionization was achieved by using two different laser systems (different wavelengths)

and high selectivity was achieved in both techniques.

The operation of the laser system (excimer and dye-laser) used in these project was discussed in detail. In LEI, laser ionization was demonstrated by collecting the current (by means of applying an electric field) generated by the creation of the charged particles in the flame. Selectivity was shown and the influences of both the electric field and the electrode gap were investigated, and a calculation was made to show that high efficiency can be achieved by using optical methods.

Time-of-flight mass spectroscopy offers a linear two-stage acceleration and a 77 cm field-free region for separation of isotopic masses. The observed time-of-flight signals were correlated with flight times for indium isotopic masses. In TOF mass spectrometry, the time-of-flight of the ions generated was calculated and also measured. The poor performance of the detector (MCP) made it impossible to demonstrate selective ionization conclusively, because we were not able to identify the exact time-of-flight of the indium atoms.

5.2 Future work

With the exception of functioning MCP detectors, a system for time-of-flight measurement and production of atomic beams was built. The next step will be to obtain new MCPs to allow accurate time-of-flight measurements. Now, in principle, different types of measurements can be performed, such as obtaining accurate isotopic masses and nuclear information using optical properties. Once we master studying stable nuclides, we can take it further by studying rare nuclides produced in nuclear reactions using the demonstrated nuclear selectivity.

Appendix A

Preparatory Experiments

At the beginning this project, a series of different experiments was conducted. The aim of doing these experiments was to enhanced my knowledge on data analysis and to learn more about laser physics. Some of the experiments conducted used the same optical instruments that are used inside the resonator cavity of a dye-laser: such experiments include the use of a diffraction grating and application of a grating. The purpose of doing these experiment was to get a clear understanding on the operation of the dye-laser.

However, more experiment were conducted using quantitative and qualitative spectroscopy techniques, such as atomic absorption, atomic emission and inductive couple plasma. A Fabry-Perot interferometer was also used in experiments such as a temperature measurement of a hot plasma and Doppler temperature measurement inside of the water cooled mercury lamp by observing the spectral line. These experiments included the applications of gratings and Doppler-free spectroscopy.

A.1 Application of grating

A.1.1 Spectrometers

A.1.2 Layout of a stigmatic grating spectrometer

Czerny-Turner design

In principle, the Czerny-Turner spectrometer is a monochromator (an optical device that transmits a mechanically selectable narrow band of wavelengths of light from a wider range of wavelengths available at the input) because it isolates a small wavelength band from a polychromatic source. The Czerny-Turner design consists of the entrance slit, mirrors (collimating and focusing mirror), plane grating and exit slit. Within the monochromator, an image of the curved or rectangular entrance slit is transferred to the exit slit after dispersion of the wavelength components of the incident beam. The components of the Czerny-Turner device work in the following way. Light enters (see A.1) the entrance slit S_1 and strikes the parabolic collimating mirrors. The entrance slit is placed at the focal plane of collimating mirror M_1 and acts as point source for M_1 which produces a parallel beam. The grating then disperses the parallel beam produced by the collimating mirror towards the focusing mirror M_2. The dispersed beam is focused in the focal plane producing an image of the entrance slit. Because the diffracted beam of any given wavelength is incident on the focusing element at a specific angle, then each wavelength is focused to a slit image at a different position on the focal plane. The exit slit S_2 placed in the focal plane of the focusing mirror therefore isolates a particular wavelength interval.

To select another wavelength in the monochromator, the grating is rotated to bring the different wavelength band through the exit slit. Changing the angle of incidence also change the diffraction angle.

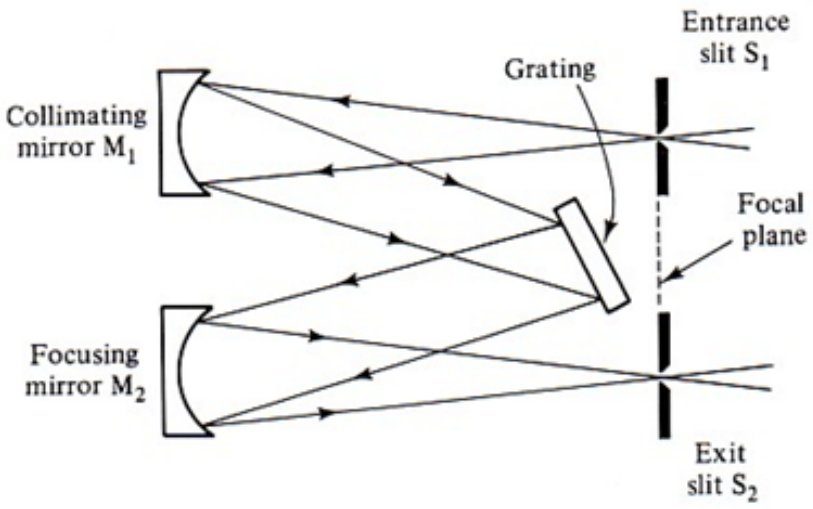

FIG. A.1. Schematic of Czerny-Turner design

A.1.2.1 Ocean Optics spectrometer design.

In the Ocean Optics spectrometer the size of the entrance aperture helps to determine how much light enters the optical bench and it is this factor that determines the optical resolution.

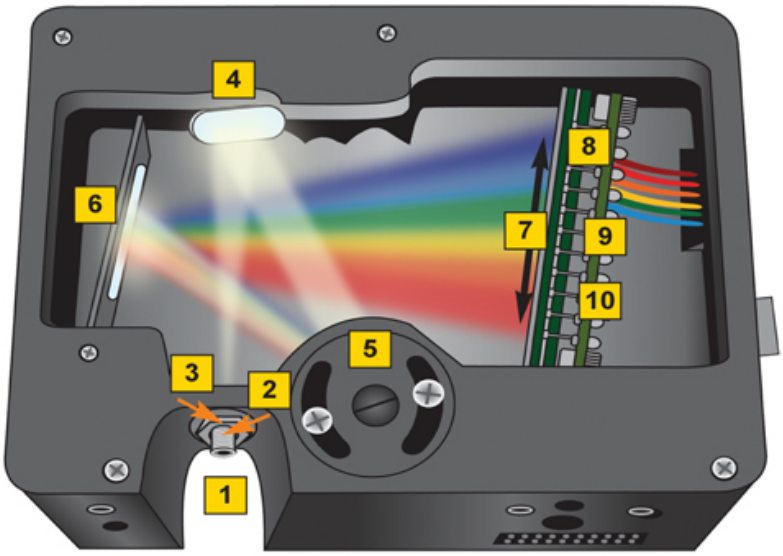

FIG. A.2. An Ocean Optic spectrometer [39].

The light from a fibre enters the optical bench through position 1 and passes through the installed entrance slit. The collimating mirror (4) is matched to the numerical aperture of the optical fibre, and then light reflects from this mirror, as a collimated beam towards the grating (5). The grating can be rotated to select the starting wavelength that has been specified. The grating is fixed in position but it can be rotated to a new fixed position if a separate wavelength region is to be studied. The focusing mirror (6) focuses the first-order spectra onto the detector plane (7).

A.1.3 Characteristics of grating spectrometers

A.1.3.1 Spectral line composition

Atoms can exist in different "excited" energy levels with different energies. These levels are referred as states i.e. the ground state, first excited state, second excited state etc. When atoms collide with each other they can absorb energy and be raised to an excited state, and when they de-excite from the excited state they emit radiation as photons. Each atom is associated with a number of discrete energy levels associated with electronic states. When atomic emission or absorption spectra are recorded, narrow spectral lines are obtained. The width of the line obtained is mainly determined by the properties of the spectrometer employed (slit function and spectral band pass) and to a lesser extent by the atomic system. With a very high resolution monochromator the actual width and profile of the atomic spectral line can be recorded. The line width obtained is the result of a variety of line broadening phenomena and these processes result in the spectral line profile [40]. If we consider a two-level system undergoing an excitation and de-excitation process, then because of the absorption and emission from the radiation field and collision processes, the excited state and the ground state have lifetimes and this gives rise to uncertainties in the energy of both states, according to the Heisenberg uncertainty principle

$$\Delta E \Delta t \approx \hbar \tag{A.1}$$

The frequency (ν) of the emitted or absorbed photons or radiation can be determined by

$$\nu = \frac{E_{exc} - E_{gr}}{h} \tag{A.2}$$

The uncertainties in energies of the states give rise to the frequency distribution of a photon. For the upper excited states, lifetime is determined by the radiative process (spontaneous and stimulated emission) and collision deactivation. The radiative lifetime results in the natural broadening, and broadening is also caused by collision deactivation of the excited state. The collision may also leave atoms in a different energy state or the same state. Broadening caused by collisions increases with an increase in concentration of the collision partners and this broadening may also be referred to as pressure broadening [24]. Since atoms are in motion, they are subjected to Doppler broadening which results from the statistical distribution of the velocity of the emitting or absorbing atoms along the observation path. The Doppler effect causes a statistical distribution in the frequency observed that is directly related to the velocity distribution [24].

A.1.3.2 Angular Dispersion

The angular dispersion of the grating can be obtained by differentiating the grating formula with respect to the wavelength and the grating formula is given by [41]

$$m\lambda = dsin\theta \tag{A.3}$$

where d is the grating constant, m is the order of diffraction, λ is the wavelength and the angle θ is the angle of the dispersed wavelength. Then the angular dispersion is given by

$$\frac{d\theta}{d\lambda} = \frac{m}{dcos\theta} \tag{A.4}$$

If the grating is operating at small angles of diffraction, then $cos\theta$ is only weakly dependent on wavelength, thus $\frac{d\theta}{d\lambda}$is nearly independent of wavelength. If we have a high order of diffraction m and a small grating constant d, then the angular dispersion will be large [41].

A.1.3.3 Linear and reciprocal linear dispersion

If we multiply the angular dispersion with the focal length f of the spectroscope then we obtain the linear dispersion, which is given by

$$\frac{dx}{d\lambda} = \frac{fm}{dcos\theta} \tag{A.5}$$

This equation tells us how far apart the two wavelengths are separated in the focal plane, where f is the focal length of the focusing element. The linear dispersion is expressed in units of mm.nm^{-1}. The reciprocal linear dispersion is the inverse of the linear dispersion and it represent the wavelength interval (nm) contained in each interval of distance (mm) along the focal plane. The reciprocal linear dispersion is given by

$$\frac{d\lambda}{dx} = \frac{dcos\theta}{fm} \tag{A.6}$$

One of the drawbacks of gratings is spectral overlapping. From the equation (A.3) it is clear that for a specific diffracting angle θ and different order m_i

$$m\lambda = \text{constant} = m_1\lambda_1 = m_2\lambda_2 = m_3\lambda_3 \tag{A.7}$$

Which means λ_1 , λ_2 , λ_3 will overlap and lead to direct interference. To observe only one wavelength the others have to be blocked with a filter that allows only the wanted wavelength through (see figure A.3).

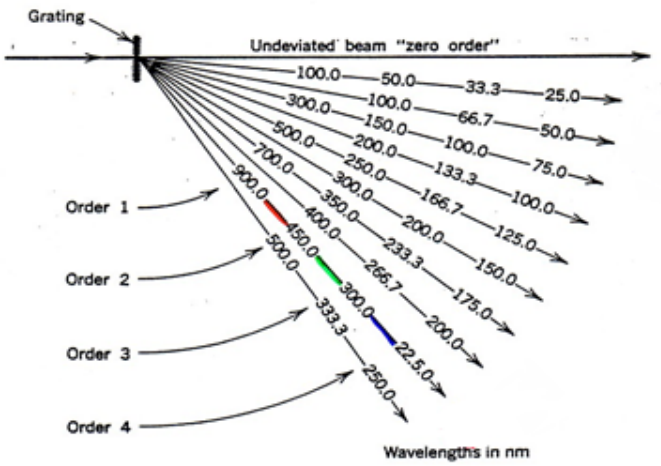

FIG. A.3. Spectral overlapping.

A.1.4 Dye Laser

A.1.4.1 Laser cavity design

A diffraction grating is used in the laser system to perform a number of functions such as to tune the lasing wavelengths and to narrow the linewidth in the laser. In order to tune the laser to a wavelength with a high gain, a grating is used at one end of the resonator cavity. A grating is used because it disperses the wavelengths in the laser, and it can be oriented so that the desired wavelength propagates back into the lasing medium. The design of the dye-laser cavity is given in figure 3.3

Diffraction gratings can be used for wavelength selection, since gratings are generally superior in terms of large dispersion and wavelength-resolving power. The use of the beam expander increases the number of grooves illuminated by the laser light leading to narrower lines and also reduces the light intensity on the grating, preventing damage to the coating on the grating surface [41].

A.1.4.2 Role of the grating in dye laser performance

As mentioned above, the grating has two functions. Firstly, by orientation it selects the wavelength that forms a standing wave in the oscillator. Secondly, its multiple illuminated grooves will narrow the spectral line produced by the dye laser.

A.1.5 Diode Lasers

A.1.5.1 External-cavity diode laser grating and mirror designs

The external cavity of a diode laser is a semiconductor laser on a laser diode chip which typically has one end anti-reflection-coated and the laser resonator is completed with a collimating lens and an external mirror. They are often used for their single-mode operation and spectral tunability. Tunable external cavity diode lasers use the diffraction grating to select the wavelength of an element in the external resonator. The longer resonator increases the damping time of the inter-cavity light and thus allows for lower phase noise and smaller emission line width. The diffraction grating acts as a filter to reduce the line width so that the line width of the external cavity diode laser is below 1MHz. They are also called grating-stabilized diode lasers. The diode laser is also referred to as a tunable laser because it is a very important tool in the field of precision laser spectroscopy. Diode lasers are increasingly taking over due to their small size, high efficiency, high power, and reliability. They are available in a wide range of the visible and infrared spectrum. The following three figures represent the external cavity laser grating and cutaway views of the external cavity and the bottom is shown in (a) while the side in shown (b).

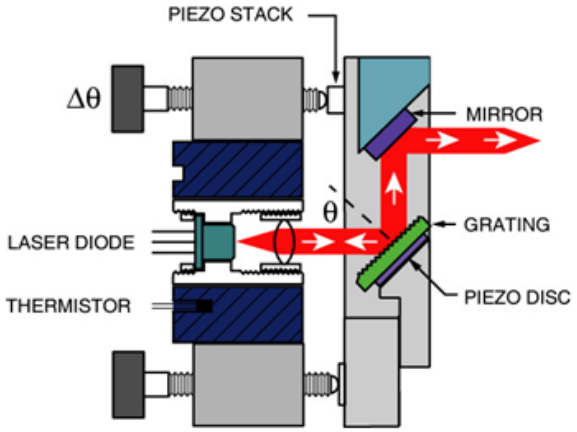

(a)

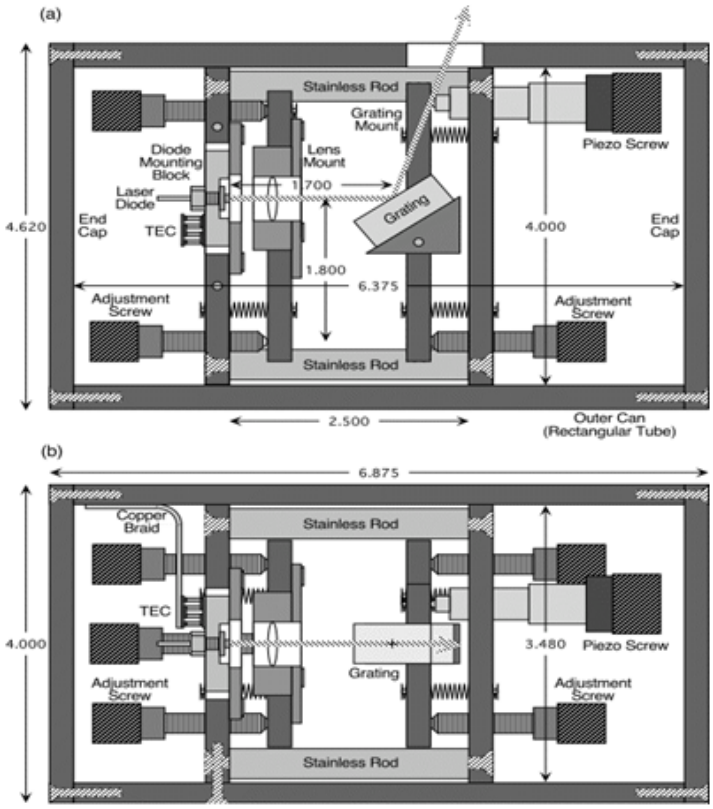

(b)

FIG. A.4. External-cavity diode laser grating and mirror designs [42].

A.2 Doppler-Free Spectroscopy

A.2.1 Aim

The aim of the experiment is to investigate the Doppler-free spectroscopy of rubidium atoms with an understanding of Doppler broadening and saturated absorption spectroscopy, and also to gain hands-on knowledge and experience in designing and setting up an experiment from scratch.

A.2.2 Introduction and physical principle

The motion of atoms creates the Doppler shifts in absorbed or emitted radiation. The spectral lines of those atoms are said to be Doppler broadened since the frequency of the absorbed or emitted radiation depends on the atomic velocities. Doppler broadening causes the individual spectral lines to be unresolved. If atoms are moving away or towards the laser they absorb radiation at different frequencies, i.e. blue or red respectively. If atoms are at rest relative to the source (laser) they absorb radiation at a frequency ν_o, where ν_o is the atomic resonance frequency when the atom is at rest relative to the laser frame. If atoms are moving towards the laser, they will absorb radiation at a frequency less than ν_o and it they are moving away from the laser they will absorb radiation at a frequency larger than ν_o. The probability of atoms having a particular velocity is given by the Maxwell-Boltzmann distribution [43, 44].

The group of atoms that interact with the pump beam is that group which counter-propagates along this beam with a requisite velocity that tunes the beam and atoms into resonance. The pump beam burns a significant hole in its group but the probe beam (because of its low intensity) causes negligible redistribution within the group. If the pump and probe beams interact with the same group of atoms, then the pump beam proceeds to depopulate this group and the probe beam finds that there are fewer atoms than in nearby group. Since the atoms are not stationary they are moving with some velocity and that velocity depends on the excitation process of changing the population in two ways, by hyperfine pumping and saturation. Hyperfine pumping is optical pumping of the atom between the hyperfine levels of the $5^2S_{1/2}$ state.

The crossover appears midway between any two transitions that have the same lower level and two different excited levels. Because the two beams can excite atoms to different excited states, when the laser is tuned to the frequency midway between two transitions, atoms with a particular velocity can simultaneously be in resonance with the saturating and probe beam, and this leads to saturated absorption, i.e. those atoms which are moving towards the probe beam with a velocity that gives Doppler shift equal to half the difference in frequency between the two transitions will "see" the probe beam shifted into the resonance with a high frequency transition. This shift will make the pump beam frequency just right to excite these atoms to the lower frequency transition and the absorption is saturated in two complementary classes of atoms moving into opposite directions at the appropriate speed [44].

Hyperfine structure of Rb atom

The hyperfine splitting of rubidium atoms arises from the coupling of the electronic and nuclear angular momenta. The interaction between the atomic electron and the nucleus consists of a magnetic interaction and an electric interaction. The magnetic interaction arises from the interaction between the magnetic dipole moment of the nucleus and the magnetic field created by the motion of the atomic electrons. The electric interaction is created by the interaction of the electric quadrupole moment of the nucleus and the gradient of the electric field of the orbiting electron.

The ground-state electron configuration of rubidium is

$1s^2; 2s^2; 2p^6; 3s^2; 3p^6; 3d^{10}; 4s^2; 4s^6; 5s^1$. The single $5s^1$ electron outside of the closed shell has an energy-level structure that resembles the hydrogen atom, which gives the ground state of $5^2s_{1/2}$ and in its first excited state the single electron become a $5s^1$ electron. The resulting excited states are $5^2s_{1/2}$ (lower) and $5^2s_{3/2}$ (higher) as shown in the following figure A.6.

Rubidium atom has two natural occurring isotopes, ^{87}Rb (28% abundance and spin (I)= 3/2) and ^{85}Rb (72% abundance and spin(I)=5/2). We are studying structure associated with the $5^2P_{3/2}$ to $5^2S_{1/2}$ transition in Rb-87 as shown in figure A.6. The spin-orbit interaction involves spin (S) and orbital (L) angular momenta that give rise to total angular

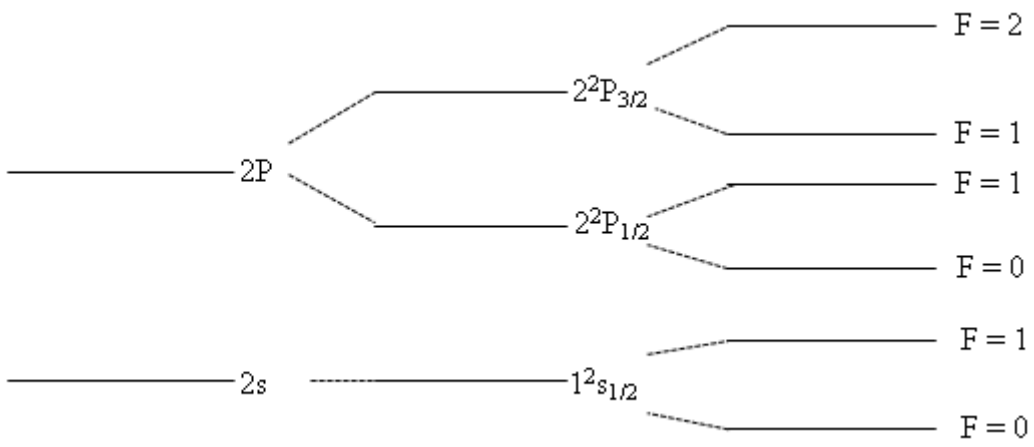

FIG. A.5. Electronic structure of Hydrogen atom.

momentum J, given by $J = S+L$, where J and I interact (couple) to give rise to new total angular momentum F given by $F = J + I$ and this new angular momentum is restricted by the sum and difference of J and I as follows $|J - I| \leq F \leq |J + I|$

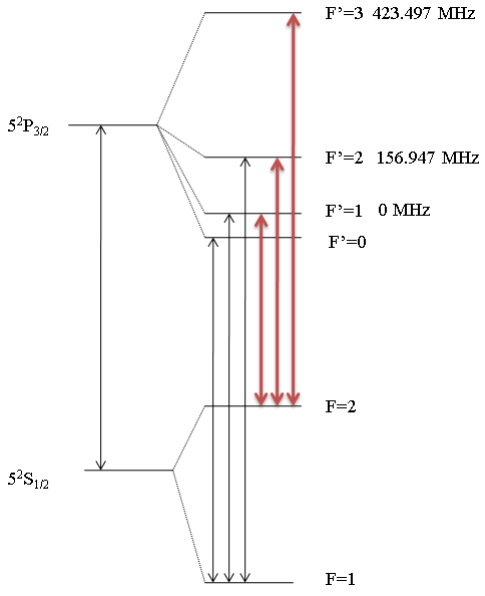

FIG. A.6. Hyperfine structure of a Rb atom and relative crossover line.

The selective saturation of molecular transition can be used to produce Doppler-free spectra. The collection of gas-phase atoms are absorbing at different frequencies of laser radiation because of the Doppler effect. Atoms moving away from the source (laser beam) absorb a lower frequency than atoms moving toward the source (laser beam). The absorption of such lines produces the inhomogeneous broadening because different atoms are responsible for different parts of the absorption line. If any frequency within the absorption line could excite all atoms with equal probability, then that line would be called homogeneous broadening. Because the Doppler width is small in many cases where a laser is used to cross the atomic or molecular beam, then it produce homogeneous broadening

A.2.3 Experimental setup and method

The experimental setup was constructed according to figure A.7. The beams (probe and pump) are arrange in such a way that they propagate in opposite directions and they overlap as they pass through the target (rubidium cell) as shown in figure A.7. One beam is called the pump beam which is more intense and the other two beams are called the probe beams and are less intense (1/10 less intense).

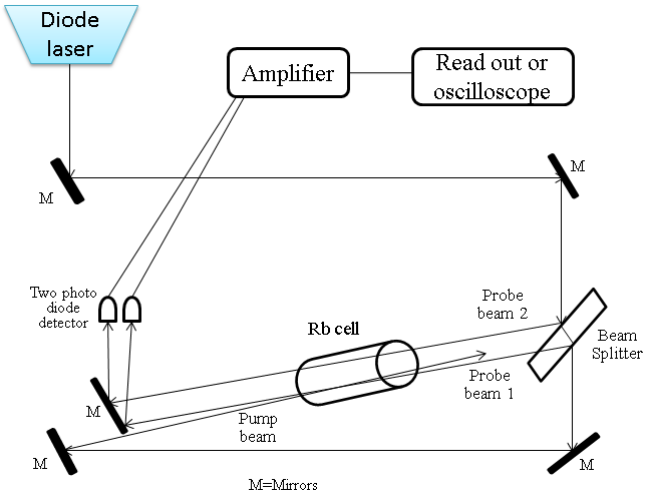

FIG. A.7. Schematic setup of Doppler-free spectroscopy.

The laser frequency is scanned back and forth over the transition frequencies of Rb. The intensities of the two probe beams are measured by separate photo-diodes and the two signals are subtracted. The resulting spectrum is displayed on an oscilloscope.

A.2.4 Results and discussion

With the apparatus set up as shonw in figure A.7, above, the saturation absorption spectrum was recorded as follows. The two probe beams passed through the rubidium cell from right to left and they were separately detected by two photo-diodes. The photo-diodes form a balanced photo-detector. The pump beam passed through the rubidium cell from left to right. In the rubidium cell there is a region where the pump beam and one probe beam overlap and they interact with the same group of atoms. The probe beam that is overlapping is referred to as the first probe beam and the other one as the second. The signal from the second probe beam will be a not affected by the pump beam (a single propagation wave is incident on a sample) where the spectral lines are Doppler broadened and this Doppler broadened spectral line is observed or obtained by blocking both the pump and the first probe beams. If the second probe beam only is blocked, the signal will be affected by the pump beam (two opposite propagating beam interact with a same sample) and the signal will be of saturation absorption spectroscopy on the Doppler broadened line. If the two signals are subtracted the Doppler broadening lines cancel out and the hyperfine structure remains. The two photo-diodes are wired in such a way that their signals subtract and the signal is Doppler-free. The pump beam changes the population of the atomic states and the probe beam detects those changes.

In the following spectrum the first peak on the left represents the $F = 2$ to $F^{'} = 3$ transition and the second and the third peak represents the crossover, the fourth represents the $F = 2$ to $F^{'} = 2$ transition and the fifth represents the crossover peak, while the sixth represents the $F = 2$ to $F^{'} = 1$ transition.

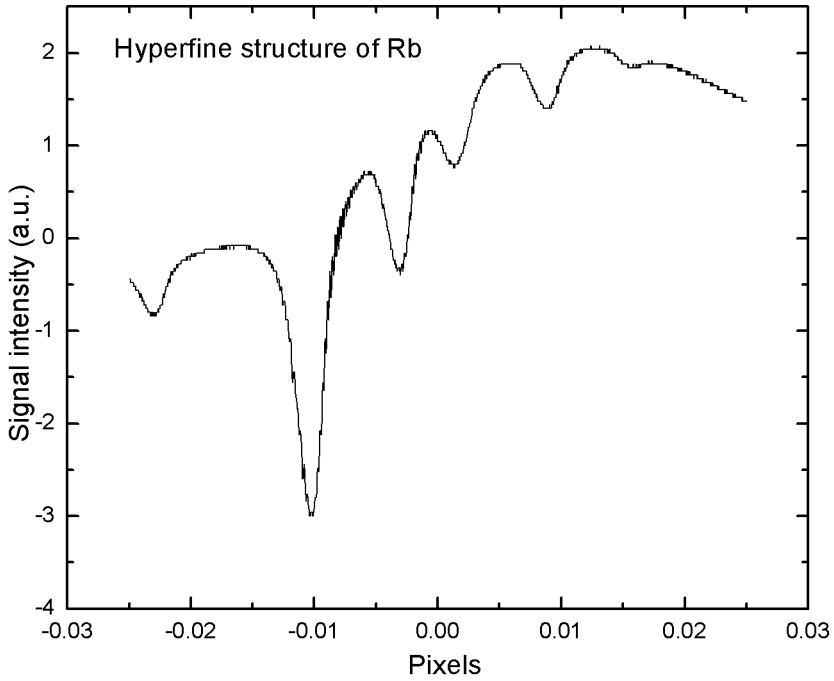

FIG. A.8. Hyperfine structure of rubidium.

The saturated absorption spectroscopy was calibrated using the relative frequency, the x scale was calibrated with the relative frequency of the real peaks shown in figure A.8, and the following table represents the calibration information. The relative frequency was calculated by estimating that the transition from $F = 2$ to $F^{'} = 1$ (first transition) is zero, and the other ones are just the difference of their own states frequency

Relative frequency (MHz)	Pixel
0	0.015473
156.947	0.001453
423.576	-0.02315

TABLE. A.1. Frequency of the crossover line.

The following plot represents the calibration curve obtain from the real frequency of rubidium-87: the peak positions in pixels are plotted against the relative frequency of these pixels. After compiled, data were linear fitted to obtain the equation of the calibration curve in terms of $y = mx + c$.

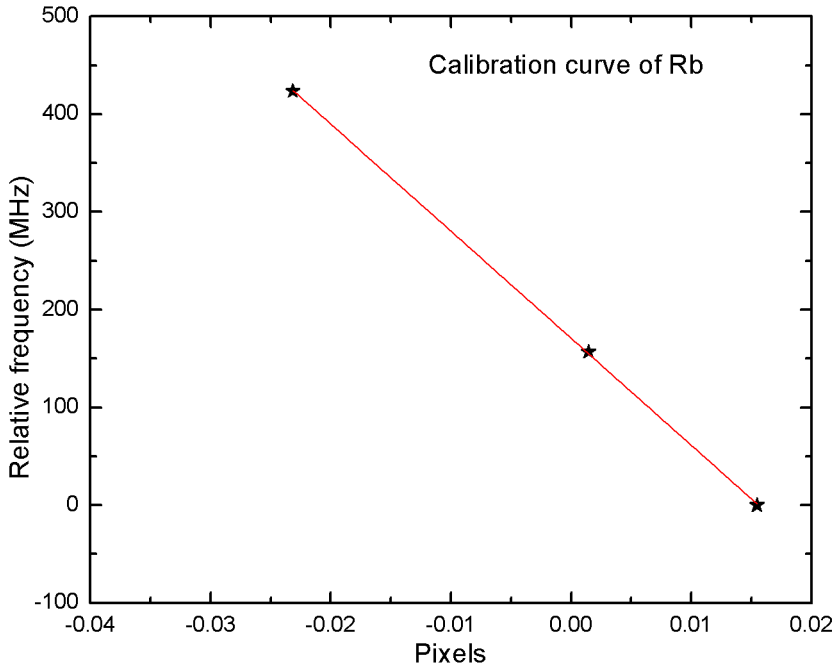

FIG. A.9. Calibration curve of Rb atom obtained from the splitting.

The equation obtained for the above plot is as follows

$$y = -10952.289x + 170.786 \tag{A.8}$$

where x represent the pixels in arbitrary units and y represent the relative frequency in MHz. The following spectrum was then obtained after fit the equation to the data (A.8) against the data obtained from the experiment. The graph now represents the hyperfine structure Rb in terms of frequency.

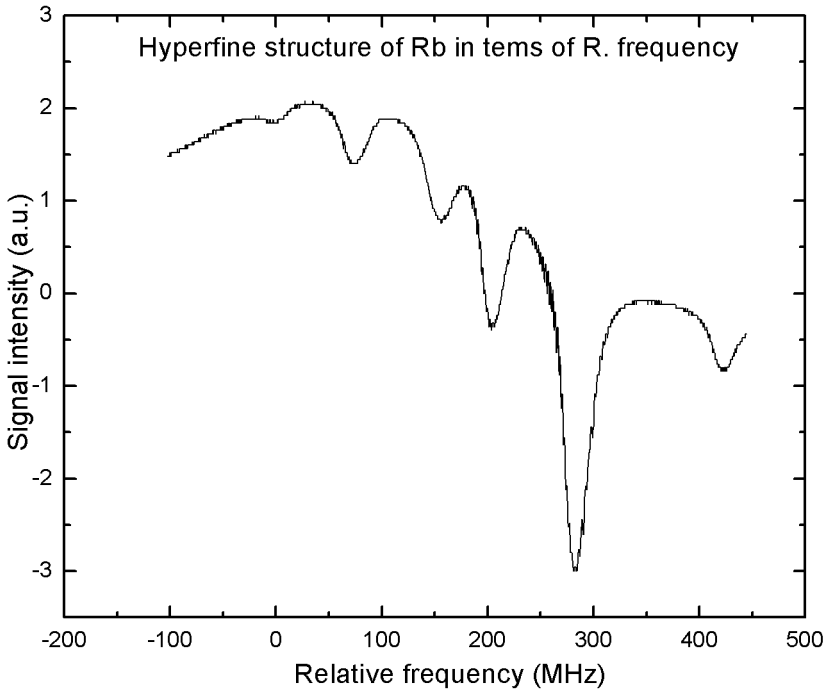

FIG. A.10. Hyperfine structure of rubidium in terms of relative frequency.

A.2.5 Conclusion

The aim of the experiment was achieved since we were successful in setting up the experimental apparatus for Doppler-free spectroscopy as shown in figure A.7 and we were able to get the Doppler broadened spectrum if one probe beam interacts with atoms and the Doppler-free spectrum with hyperfine structure was observed if the second probe beam is interacting with same sample as the pump beam (overlapping), and if those two spectral lines were subtracted we were left with the Doppler-free spectrum as shown in figure A.8. After calibrating the spectrum we able to obtain the spectrum in terms of relative frequency as shown in figure A.10. This technique of obtaining the Doppler-free spectrum is important because it avoids the Doppler broadening which can influence our result. It was understood that the hyperfine spectrum cannot be obtained if we cool the rubidium vapour cell because cooling will decrease the pressure and this results in poor absorption by the atoms.

Bibliography

[1] L. Biasetto A. Andrighetto and M. Manzolaro. Production of high-intensity RIB at SPES. *Nuclear Physics A*, 834:754–757, 2010.

[2] M. Huyse. The why and how of radioactive-beam research. *Lect. Notes Phys*, 651:1–32, 2004.

[3] Robert Bark. Radioactive-ion beam facility at iThemba LABS. 2011.

[4] A. Bonaccorso and G. Prete. EURISOL: an European Isotope Separation On-Line radioactive-ion beam facility. *Journal of Physics: Conference Series*, 168:1–15, 2009.

[5] P. Van Duppen. Isotope separation on line and post acceleration. *Lect. Notes Phys*, 700:37–77, 2006.

[6] B. Cheal and K. T. Flanagan. Progress in laser spectroscopy at radioactive ion beam facilities. *Journal of Physics G: Nuclear and Particle Physics*, 37:1–38, 2010.

[7] D.K. Olsen. Opportunities with accelerated radioactive ion beams. *Nuclear Instruments and Methods in Physics Research*, A328:303–320, 1993.

[8] U. Koster. Resonance ionization laser ion sources. *Nuclear Physics A*, 701:441–451, 2002.

[9] J. Lassen J.P. Lavoie, P. Bricault and M.R. Pearson. Segmented linear radiofrequency quadrupole / laser ion source project at TRIUMF. In *Trapped Charged Particles and Fundamental Physics*, 2007.

[10] Vladilen S. Letokhov. *Laser Photoionization Spectroscopy.* Academic Press, inc., 1987.

[11] V. S. Letokhov. Laser spectroscopy: Multiphoton and multistep method. *Optics and Laser Technology*, pages 247–256, 1978.

[12] G. Samuel Hurst and James E. Parks. Methods and applications of resonance ionization spectroscopy. *Experimental Methods in the physical sciences*, 29B:171–190, 1996.

[13] Iain Moore. Resonant laser ionization, spectroscopy and IGISOL-4. In *Resonance Laser Separation Workshop,JINR, Dubna*, 6 -7/12/2011.

[14] V.N. Fedosseev U. Koster and V.I. Mishin. Resonant laser ionization of radioactive atoms. *Spectrochimica Acta Part B*, 58:1047–1068, 2003.

[15] Piet Van Duppen. Laser ion sources for on-line isotope separators. *Nuclear Instruments and Methods in Physics Research B*, 126:66–72, 1997.

[16] S. Franchoo M. Hyse P. V. Duppen P. Van Den Bergh L. Vermeeren J. Wauters A. Wohr J. Gentens J. Szerypo I. Reusen J. Andrzejewski J. Szerypo Y. Kudryavtsev, N. Bijness. Beams of short lived nuclei produced by selective laser ionization in a gas cell. *Nuclear Instruments and Methods in Physics Research B*, 114:350–365, 1995.

[17] M. Huyse J. Gentens P. Van den Bergh Yu. Kudryavtsev, M. Facina and P. Van Duppen. Beams of isotopes produced at LISOL by laser ionization after thermalization of energetic ions in a gas cell. *Nuclear Instruments and Methods in Physics Research B*, 204:336–342, 2003.

[18] Ulli Koster. Ionization and chemical separation of radioactive isotope. In *Stellenbosch summer school*, 2008.

[19] Gianfranco Prete. A second generation of ISOL facility. In *The second meeting of the union for compact accelerator driven neutron sources, Bloomington*, 5-8/07/2011.

[20] Anthony F. State. The calculation of photoionization cross section. *Research papers in physics and astronomy*, pages 2–27, 1988.

[21] D. V. Karaivanov Yu. P. Gangrskii. Measurement of ionizing radiations: Laser ionization spectroscopy based on a beam of charged cyclotron particles. *Measurement Techniques*, 41:1079–1084, 1998.

[22] Ove Axner and Halina Rubinsztein-Dunlop. Laser-enhanced ionization spectrometry in flames - A powerful and versatile technique for ultra-sensitive trace element analysis. *Spectrochimica Acta*, 44B:835–866, 1989.

[23] Ove Axner. Determination of optimum conditions for laser-enhanced ionization spectrometry in flames-I. One-step signal strength versus excitation transition. *Spectrochimica Acta*, 45B:561I–579, 1990.

[24] James D. Ingle Jr and Stanley R. Crouch. *Spectrochemical Analysis*. Prentice Hall Inc., 1988.

[25] Totaro Imasaka and Nobuhiko Ishibashi. Analytical techniques using lasers. *Prog. Quant. Electr.*, 14:131–249, 1990.

[26] G. C. Turk J. C. Travis and R. B. Green. Laser enhanced ionization spectroscopy. *Analytical Chemistry*, 54:1006A–1013A, 1982.

[27] Ingemar Magnusson. On the signal collection in laser enhanced ionization spectrometry. *Spectrochimica Acta*, 42B:I 113–1123, 1987.

[28] I. I. Vlasov and N. V. Chekalin. A new approach to the determination of the ionization yield of atoms by laser-enhanced ionization. *Spectochemica Acta*, 48B:597–603, 1993.

[29] Denis Boudreau and Jean-Francois Gravel. Laser-enhanced ionization: recent developments. *Trends in analytical chemistry*, 20:20–27, 2001.

[30] William T. Silfvast. *Laser Fundamentals (Second Edition)*. Cambrige University Press, 2004.

[31] Peter W. Milonni and Joseph H. Eberly. *Laser Physics*. John Wiley and Son, 2010.

[32] Muhammad Saleen. *Laser Assisted Isotopic Studies Using Time of Flight Mass Spectroscopy*. PhD thesis, Quaid-i-Azam University, Pakistan, 2006.

[33] Michael Guilhaus. Principles and instrumentation in time-of-flight mass spectrometry. *Journal of Mass Spectrometry*, 30:1519–1532, (1995).

[34] W.C. Wiley and I.H. Mclaren. Time-of-flight mass spectrometer with improved resolution. *Review of Scientific Intruments*, 26:1150–1157, 1955.

[35] *Photomultiplier Tubes.* Hamamatsu Photonics K.K, 2006.

[36] Joseph Lasislas Wiza. Microchannel plate detector. *Nuclear Instruments and Methods*, 162:587–601, 1979.

[37] Hamamatsu. MCP and MCP assembly selection guide. Technical report, 2009.

[38] E.B. Soloman. A resonance ionization spectroscopy/resonance ionization mass spectroscopy data service. IV-data sheets for Be, In, Li, K, Rb, Ag, Ti and V and update of the data sheet for Ni. *Spectochemica Acta*, 48B:1139–1203, 1993.

[39] www.chem.orst.edu/courses/ch361-460/ch461/ocean optics spectrometer.htm.

[40] Atomic emission spectroscopy. Technical report, University of Stellenbosch, 2003.

[41] Christopher Palmer. *Diffraction Grating Handbook (5th Edition).* 2002.

[42] http://optics.ph.unimelb.edu.au/atomopt/diodes.html.

[43] Philip J. Ilten. Doppler-free spectroscopy. Technical report, MIT Department of Physics, 2005.

[44] Philip J. Ilten. Doppler-free spectroscopy of rubidium. Technical report, MIT Department of Physics, 2007.

[45] V. Tikhonov A. Jokinen, A.H. Evensen. Selective laser ionization of radioactive Ni-isotopes. *Nuclear Instruments and Methods in Physics Research B*, 126:95–99, 1997.

[46] Wallace R. Brode. *Chemical spectroscopy.* John Wiley and Son, 1958.

[47] D. P. Eastman D.H. Frank. Hyperfune structure of some Hg I lines. *Optical Society of America*, 50:1045–1052, 1960.

[48] C. A. Busse F. Geiger and R. I. Loehrke. The vapor pressure of indium, silver, gallium, copper, tin, and gold between 0.1 and 3.0 bar. *International Journal of Thermophysics*, 8:425–436, 1986.

[49] Per Hakansson. An introduction to the time-of-flight technique. *Brazilian Journal of Physics*, 29:422–427, 1999.

[50] Eugene Hecht. *Optics (4th Edition)*. Addison Wesley, 2002.

[51] Laser Research Institute. Short course, Introdiction to lasers. Technical report, University of Stellenbosch, 2003.

[52] B. W. Smith L. P. Hart and N. Omenetto. Laser induced stepwise and two-photon ionization studies of strontium in the air acetylene flame. *Spectrochimica Acta*, 40B:1637–1649, 1985.

[53] Mats Lindroos. Review of ISOL type Radioactive-Ion beam facilities. In *European Particle Accelerator conference*, 2004.

[54] Jan Van Roosbroeck. *Systematic Nuclear-Structure Study of Even-Mass Zn and Cu Isotopes between N=40 and 50.* PhD thesis, Katholieke Universiteit Leuven, 2002.

[55] U. Koster V.N. Fedosseev and L. Weissman. Atomic spetroscopy studies of short-lived isotopes and nuclear isomer separation with ISOLDE RILIS. In *14th International Conference on Eletromagnetic Isotope Separators and Techniques Related to their Application*, 2002.